

1 **Abstract**

2 During the Last Interglacial (LIG, ~130–115 kiloyear (kyr) before present (BP)), the northern high
3 latitudes were characterized by higher temperatures than those of the late Holocene and a lower
4 Greenland Ice Sheet (GIS). However, the impact of a reduced GIS on the global climate has not yet
5 been well constrained. In this study, we quantify the contribution of the GIS to LIG warmth by
6 performing various sensitivity studies based on equilibrium simulations, employing the Community
7 Earth System Models (COSMOS), with a focus on height and extent of the GIS. We present the first
8 study on the effects of a reduction in GIS on the surface temperature (TS) on a global scale and
9 separate the contribution of different forcings to LIG warmth. The strong Northern Hemisphere
10 warming is mainly caused by increased summer insolation. Reducing the height by ~1300 m and the
11 extent of the GIS does not have a strong influence during summer, leading to an additional global
12 warming of only +0.24°C. The effect of a reduction in GIS is strongest during local winter, with up to
13 +5°C warming and with an increase in global average temperature of +0.48°C.

14 In order to evaluate the performance of our LIG simulations, we additionally compare the simulated
15 TS anomalies with marine and terrestrial proxy-based LIG temperature anomalies derived from three
16 different proxy data compilations. Our model results are in good agreement with proxy records with
17 respect to the warming pattern, but underestimate the reconstructed temperatures, suggesting a potential
18 misinterpretation of the proxy records or deficits of our model. However, we are able to partly reduce
19 the mismatch between model and data by additionally taking into account the potential seasonal bias of
20 the proxy record and/or the uncertainties in the dating of the proxy records for the LIG thermal
21 maximum. The seasonal bias and the uncertainty of the timing are estimated from new transient model
22 simulations covering the whole LIG. The model-data comparison improves for proxies that represent
23 annual mean temperatures when GIS is reduced and when we take into account the local thermal
24 maximum during the LIG (130-120 kyr BP). For proxy data that represent summer temperatures,
25 changes in GIS are of minor importance for sea surface temperatures. However, the temperature change
26 over Greenland in the reduced GIS simulations seems to be overestimated as compared to the local
27 data, which could be related to the interpretation of the recorder system and/or the assumptions of GIS
28 reduction. Thus, the question regarding the real size of the GIS during the LIG has yet to be answered.

29 **1. Introduction**

30 One important application of atmosphere–ocean general circulation models (AOGCMs) is the
31 computation of future climate projections (Collins et al., 2013; Kirtman et al., 2013), which allow

1 insight into possible future climate states that may be notably different from present day. In order to
2 ensure the reliability of such climate projections, the climate models' ability to replicate climate states
3 that are different from the present needs to be tested (e.g. Braconnot et al., 2012; Flato et al., 2013).
4 Past time periods provide the means for evaluating the performance of general circulation models (e.g.
5 Dowsett et al., 2013; Lohmann et al., 2013; Lunt et al., 2013).

6 In particular, the simulation of interglacial climates provides an example of how models can
7 respond when strong changes in the forcing are applied (Mearns et al., 2001) and the possibility to
8 analyze the main drivers leading to an interglacial climate that was warmer than the present
9 interglacial. The Last Interglacial (LIG, ~130–115 kiloyear (kyr) before present (BP)) is considered to
10 be on average warmer than the Holocene (10–0 kyr BP) (CLIMAP Project Members, 1984; Martinson
11 et al., 1987; Kukla et al., 2002; Bauch and Erlenkeuser, 2003; Felis et al., 2004; Kaspar et al., 2005;
12 Jansen et al., 2007; Turney and Jones, 2010; Masson-Delmotte et al., 2013). Model simulations indicate
13 a pronounced warming during boreal summer in northern high latitudes (Harrison et al., 1995; Kaspar
14 et al., 2005; Otto-Bliesner et al., 2006; Lohmann and Lorenz, 2007; Stone et al., 2013). Proxy records
15 located in the Northern Hemisphere indicate also that LIG climate is characterized by temperatures that
16 are several degrees Celsius above preindustrial values (Kaspar et al., 2005; CAPE Last Interglacial
17 Project Members, 2006; Turney and Jones, 2010; Mckay et al., 2011). Winter in high latitudes is
18 considered to be warmer during the LIG due to sea ice feedbacks (Montoya et al., 2000; Kaspar et al.,
19 2005; Yin and Berger, 2010). One cause for LIG summer warmth was increased summer insolation at
20 middle to high latitudes. Greenhouse gas (GHG) concentrations during the LIG were similar to the
21 preindustrial (PI).

22 Studies based on reconstructions and climate model simulations suggest a partial or complete
23 absence of the Greenland Ice Sheet (GIS) during the LIG, and that the sea level was higher than the PI
24 (Veeh, 1966; Stirling et al., 1998; Cuffey and Marshall, 2000; Otto-Bliesner et al., 2006; Overpeck et
25 al., 2006; Jansen et al., 2007; Kopp et al., 2009, 2013; Alley et al., 2010; van de Berg et al., 2011;
26 Robinson et al., 2011; Dutton and Lambeck, 2012; Quiquet et al., 2013; Church et al., 2013; Stone et
27 al., 2013), while a more recent study based on ice core data proposes only a modest GIS change (i.e.
28 equivalent to a contribution to sea level rise of ~2 m, NEEM Community members, 2013). An increase
29 in sea level during the LIG is estimated to be of about 7 m (Kopp et al., 2009; Dutton et al., 2015), with
30 a possible contribution of 3 to 4 m from Antarctica (Sutter et al., 2015). The contribution of a partially
31 melted GIS to LIG sea level rise is however not yet well determined; various studies suggest a sea level

1 rise due to meltwater from Greenland of +0.3 to +5.5 m (Cuffey and Marshall, 2000; Tarasov and
2 Peltier, 2003; Lhomme et al., 2005; Otto-Bliesner et al., 2006; Colville et al., 2011; Quiquet et al.,
3 2013; Stone et al., 2013).

4 Existing studies on the effects of a reduced GIS during the LIG have been centered mostly on the
5 Northern Hemisphere and focused on implications related to sea level rise (Stone et al., 2013) and
6 Atlantic Meridional Overturning Circulation (AMOC) (Bakker et al., 2012). The studies by Bakker et
7 al. (2012) and Stone et al. (2013) assume a relatively modest reduction of the GIS and find a mismatch
8 between the simulated and the proxy-based temperature anomalies with respect to PI (CAPE Last
9 Interglacial Project Members, 2006). Otto-Bliesner et al. (2006) find that a GIS elevation reduced by
10 500 m leads to a pronounced warming of up to +5°C in middle to high latitude summer. However, they
11 find as well a mismatch between model and data, with the model underestimating the temperature
12 anomaly indicated by the proxy record. In an LIG study based on transient climate model simulations
13 performed with an earth system model of intermediate complexity, Loutre et al. (2014) find that
14 changes in the Northern Hemisphere ice sheets configuration (extent and albedo) have only a small
15 impact on the climate at the beginning of the LIG. They find as well an underestimation of the
16 reconstructed temperatures by the model.

17 Other model-data comparison studies for the LIG (Lunt et al., 2013; Otto-Bliesner et al., 2013),
18 based on AOGCMs (but with no changes in GIS elevation or extent), also show an underestimation of
19 global temperature reconstructions (Turney and Jones, 2010; McKay et al., 2011). Bakker and Renssen
20 (2014), who perform an analysis of transient simulations for the LIG, provide a partial explanation for
21 the model-data mismatch, proposing that such large differences between the reconstructed and
22 simulated LIG temperatures may stem from the fact that commonly-used climate syntheses represent a
23 single time-slice assuming synchronous LIG thermal maximum in space and time. Their study suggests
24 that global compilations of reconstructed LIG thermal maximum overestimate the warming. However,
25 different studies (modelling as well as proxy-based) indicate that the maximum LIG warmth occurred
26 at different times throughout the LIG in dependence of the geographical location (Bakker et al., 2012;
27 Govin et al., 2012; Langebroek and Nisancioglu, 2014). The lack of climate synthesis for the LIG
28 going further than proposing a single snapshot on LIG maximum warmth and thus accounting for
29 asynchronous changes across the globe is due to the difficulty in building robust and coherent age
30 models for different climatic archives during the LIG (Govin et al., 2015). Recently, Capron et al.
31 (2014) propose a new climate synthesis for the high latitude regions based on a coherent temporal

1 framework between ice and marine archives. This allows for the first time to assess both the temporal
2 and the spatial evolution of the climate throughout the LIG (Capron et al., 2014).

3 Transient LIG climate simulations provide the possibility to determine when and where maximum
4 LIG warmth occurred, and whether a given record may be seasonally biased or rather represents annual
5 mean temperatures. Therefore, transient climate simulations may help to clarify the origin of the
6 disagreement between model and data. In this study, we analyze the effect of a reduced GIS on LIG
7 global climate with a focus on surface temperature (TS) at 130 kyr BP. The TS is derived from
8 equilibrium simulations performed with an AOGCM. We perform several sensitivity simulations with
9 different boundary conditions and use three different methods of reducing GIS elevation to half its
10 preindustrial elevation and/or extent. This approach enables us to determine what GIS configuration
11 has the strongest impact on the global temperature. Additionally, we assess the importance of additional
12 forcings like insolation and albedo. Furthermore, in order to validate our results, we perform a model-
13 data comparison using three different proxy-based temperature compilations by CAPE Last Interglacial
14 Project Members (2006), Turney and Jones (2010), and Capron et al. (2014). For model-data
15 comparison, we additionally consider the timing uncertainty on the maximum LIG warmth as
16 determined from our transient simulations as well as the potential seasonal bias of the proxy record.

17 **2. Data and methods**

18 **2.1 Model description**

19 The Community Earth System Models (COSMOS) consist of the general atmosphere circulation model
20 ECHAM5 (5th generation of the European Centre Hamburg Model; Roeckner et al., 2003), the land
21 surface and vegetation model JSBACH (Jena Scheme of Atmosphere Coupling in Hamburg; Raddatz et
22 al., 2007), the general ocean circulation model MPIOM (Max-Planck-Institute Ocean Model; Marsland
23 et al., 2003), and the OASIS3 coupler (Ocean-Atmosphere-Sea Ice-Soil; Valcke et al., 2003; Valcke,
24 2013) that enables the atmosphere and ocean to interact with each other. COSMOS is mainly developed
25 at the Max-Planck-Institute for Meteorology in Hamburg (Germany). The atmospheric component
26 ECHAM5 is a spectral model, which is used in this study at a horizontal resolution of T31
27 ($\sim 3.75^\circ \times 3.75^\circ$) with a vertical resolution of 19 hybrid sigma-pressure levels, the highest level being
28 located at 10 hPa. The JSBACH simulates fluxes of energy, momentum, and CO₂ between land and
29 atmosphere and comprises the dynamic vegetation module by Brovkin et al. (2009), which enables the
30 terrestrial plant cover to explicitly adjust to variations in the climate state. MPIOM is formulated on a

1 bipolar orthogonal spherical coordinate system. We employ it at a horizontal resolution of GR30
2 (corresponding to $\sim 3^\circ \times 1.8^\circ$) with 40 vertical levels. MPIOM includes a Hibler-type zero-layer
3 dynamic-thermodynamic sea ice model with viscous plastic rheology (Semtner, 1976; Hibler, 1979).
4 No flux correction is applied (Jungclaus et al., 2006). Model time steps are 40 min (atmosphere) and
5 144 min (ocean). This COSMOS configuration has been applied for the mid- and early Holocene (Wei
6 and Lohmann, 2012), glacial conditions (Gong et al., 2013; Zhang et al., 2013, 2014), the Pliocene
7 (Stepanek and Lohmann, 2012), the Miocene (Knorr et al., 2011; Knorr and Lohmann, 2014), future
8 climate projections (Gierz et al., 2015), and the LIG (Lunt et al., 2013; Pfeiffer and Lohmann, 2013;
9 Bakker et al., 2014; Felis et al., 2015; Gong et al., 2015; Jennings et al., 2015).

10 **2.2 Experimental setup**

11 As control climate, we use a PI simulation described by Wei et al. (2012). Greenhouse gas
12 concentrations and astronomical forcing of the PI simulation are prescribed according to the
13 Paleoclimate Modelling Intercomparison Project Phase 2 (PMIP2) protocol (Braconnot et al., 2007).
14 Several equilibrium simulations covering the LIG are performed using fixed boundary conditions for
15 130 and 125 kyr BP time slices. The latter simulation is performed in order to assess whether a
16 reduction in GIS at 125 kyr BP improves the agreement between the model and the three proxy
17 compilations considered in this study (CAPE Last Interglacial Project Members, 2006; Turney and
18 Jones, 2010; 125 kyr BP time slice by Capron et al., 2014). Astronomical parameters for the time slices
19 considered in this study have been calculated according to Berger (1978) and are given in Table 1. It is
20 known that one main driver for LIG climate is the Earth's astronomical parameters (Kutzbach et al.,
21 1991; Crowley and Kim, 1994; Montoya et al., 2000; Felis et al., 2004; Kaspar and Cubasch, 2007).
22 During the early part of the LIG, the axial tilt (obliquity) was higher which caused stronger summer
23 insolation at high latitudes of the Northern Hemisphere, while the low latitudes received less insolation;
24 this effect manifests in enhanced seasonality (i.e. warmer summers and cooler winters) in the early LIG
25 climate. The Earth's orbital eccentricity was more than twice the present-day value (Berger and Loutre,
26 1991), and boreal summer coincided with the Earth passing the perihelion (Laskar et al., 2004; Yin and
27 Berger, 2010).

28 Our main focus is the effects of height and extent of the GIS and of insolation changes on climate;
29 consequently, GHG concentrations are prescribed at mid-Holocene levels (278 parts per million by
30 volume (ppmv) CO₂, 650 parts per billion by volume 10 (ppbv) CH₄, and 270 ppbv N₂O, Table 1). An
31 additional simulation is performed using values for GHG concentrations proposed in the Paleoclimate

1 Modelling Intercomparison Project Phase 3 (PMIP3) for the 130 kyr BP time slice (e.g. Lunt et al.,
2 2012) and corresponding to 257 ppmv for CO₂, 512 ppbv for CH₄, and 239 ppbv for N₂O (LIG-GHG,
3 Table 1, Fig. S1). This simulation is included in the Supplementary material as a control run for the
4 GHG concentrations used in our LIG sensitivity simulations, in order to show that there is no large
5 scale impact of lower GHG concentrations relative to our LIG control simulation (Fig. S1). Another
6 LIG simulation is forced with increased CH₄ (760 ppbv) and slightly increased CO₂ (280 ppmv) in
7 order to have one LIG simulation that has identical GHG concentrations to the ones prescribed in the PI
8 simulation (Wei et al., 2012) (Table 1).

9 The size of the GIS during the LIG is not well constrained by reconstructions (Koerner, 1989;
10 Koerner and Fisher, 2002; NGRIP members, 2004; Johnsen and Vinther, 2007; Willerslev et al., 2007;
11 Alley et al., 2010; NEEM Community members, 2013). We take this uncertainty into account and
12 perform sensitivity simulations with three different elevations and two different ice sheet areas of the
13 GIS (Fig. 1). An LIG simulation with a preindustrial GIS elevation ((LIG-ctl, Table 1, Fig. 1a) is used
14 as control run for our LIG simulations, which allows us to quantify the exclusive effects of Greenland
15 elevation on climate. Four simulations are performed using a modified GIS (Table 1). We consider (1)
16 GIS lowered to half its preindustrial elevation with unchanged GIS area (LIG- $\times 0.5$, Fig. 1b); (2) a GIS
17 lowered by 1300 m (LIG-1300m); at locations where the preindustrial Greenland elevation is below
18 1300 m, we set LIG orography to zero meters, but define the ground to be ice covered and keep the
19 albedo at values typical for the GIS (Fig. 1c); (3) a GIS similar to LIG-1300m, but with albedo
20 adjustment at locations where prescribed LIG orography is zero meters (LIG-1300m-alb); at such
21 locations the land surface is defined as being ice-free and the background albedo is reduced from 0.7 to
22 0.16 (Fig. 1d), an albedo value that is typical for tundra (Fitzjarrald and Moore, 1992; Eugster et al.,
23 2000) – this simulation, in combination with LIG-1300m and LIG-ctl, allows us to separate the climatic
24 effects of a lowered and spatially reduced GIS from those of changes in albedo; (4) a simulation similar
25 to (3), but with an atmospheric concentration of CH₄ that is increased to 760 ppbv (LIG-1300m-alb-
26 CH₄, Fig. 1d); this simulation enables us to quantify the combined effect of a lowered GIS elevation,
27 changes in albedo and insolation with respect to PI.

28 Such changes in GIS elevation and extent would lead to a sea level rise of about 3 m instead of 7 m
29 for the present situation due to the rebound effect (relaxation of the lithosphere). A sea level change of
30 +3 m is in agreement with other studies that suggest an increase in sea level of 0.3 to 5.5 m during the
31 LIG as a result of GIS melting (Cuffey and Marshall, 2000; Tarasov and Peltier, 2003; Lhomme et al.,

1 2005; Otto-Bliesner et al., 2006; Carlson et al., 2008; Colville et al., 2011; Quiquet et al., 2013; Stone
2 et al., 2013). Generally, other boundary conditions of the simulations are kept at their preindustrial
3 state, except for vegetation which is computed dynamically according to the prevailing climate
4 conditions (the only equilibrium simulation that considers fixed preindustrial vegetation is LIG-GHG).

5 Furthermore, we perform one transient model simulation that covers the Holocene (8–0 kyr BP) and
6 four transient simulations of the LIG (130–115 kyr BP). The Holocene transient simulation is included
7 in this study as a control run for the LIG transient simulations, in order to assess the differences and
8 similarities between the present and last interglacial. For the LIG, we apply orography configurations
9 of LIG-ctl, LIG- $\times 0.5$, LIG-1300m-alb, and LIG-GHG, respectively. These LIG transient simulations
10 enable us to extract the temperatures at the LIG thermal maximum. The transient simulations are
11 started from a near-equilibrium state, meaning that the climate system is already adjusted to the
12 prescribed forcings, except for the ocean which needs about 3000 years in order to reach an equilibrium
13 state. Performing such long equilibrium simulations is not feasible due to the involved computational
14 effort. Each transient simulation is accelerated by a factor of ten in order to reduce the computational
15 expense. To this end, astronomical forcing is accelerated following the method of Lorenz and Lohmann
16 (2004). The astronomical parameters are calculated after Berger (1978). During the simulations, the
17 trace gas concentrations remain fixed – except for the LIG-GHG-tr, where a timeseries is prescribed
18 according to Lüthi et al. (2008) for CO₂, Loulergue et al. (2008) for CH₄, and Spahni et al. (2005) for
19 N₂O, as proposed for PMIP3. The respective values are interpolated to a 0.01 kyr resolution that
20 corresponds to the accelerated model time axis. A fixed preindustrial vegetation is considered only in
21 the LIG-GHG-tr, in the other transient simulations vegetation is computed dynamically. For the
22 Holocene run, the orography is identical to preindustrial conditions.

23 In order to determine whether TS anomalies between simulations are statistically significant or rather
24 caused by internal variability (noise), we perform an independent two-tailed Student's t test t following
25 Eq. (1). For each grid cell, it relates time averages X and standard deviations σ of model output time
26 series of two given model simulations X_1 and X_2 of a length of n timesteps, in dependence of the
27 effective degrees of freedom (DOF_{eff}). The DOF_{eff} are calculated considering the lag-1 autocorrelation
28 acf (von Storch and Zwiers, 1999):

$$29 \text{ DOF}_{\text{eff}} = n(1 - \text{acf}) / (1 + \text{acf}) \quad \text{with} \quad \text{acf} = \max(\text{acf}, 0),$$

30 meaning that the DOF_{eff} cannot be higher than 50, as the last 50 model years of each simulation are
31 used for the analysis. For each grid point from X_1 and X_2 simulations, the smaller DOF_{eff} value is used

1 for calculating the significance value with a 95% confidence interval.

$$t = \frac{\bar{X}_1 - \bar{X}_2}{\sqrt{\frac{\sigma^2(X_1)}{n} + \frac{\sigma^2(X_2)}{n}}} \quad (1)$$

2
3 Surface temperature at locations where the t test t of two data sets indicates a significance value below
4 the critical value is considered to be statistically insignificant and is marked by hatches on geographical
5 maps presented throughout this study.

6 For the analysis of time slice simulations, we define winter and summer as the mean of the 50
7 coldest and warmest months, respectively, for each grid cell, as we are mainly interested in local
8 seasons. In all performed simulations, a modern calendar is assumed. Although in reality the definition
9 of seasons changes over time due to orbital precession, taking this calendar shift into account would
10 only have a minor influence on our results since we calculate the summer and winter seasons by
11 extracting the warmest and coldest month, respectively. Maximum and minimum LIG TS are calculated
12 from the transient simulations considering the time interval between 130 and 120 kyr BP. In order to
13 filter out internal variability, a 100-point running average representing the average over 1000 calendar
14 years is applied. Maximum and minimum LIG warmth of the summer are defined as the warmest and
15 coldest average of 100 warmest months, respectively, which reflects the warmest or coldest 1000
16 summer seasons with respect to the astronomical forcing. For the maximum and minimum LIG warmth
17 of annual mean, we consider the warmest and coldest average of 100 model years, respectively. The
18 seasonality range is defined by calculating the summer maximum LIG warmth (warmest average of
19 100 warmest months of the model years) and winter minimum LIG TS (coldest average of 100 coldest
20 months of the model years).

21 **2.3 Temperature reconstructions**

22 In order to test the robustness of our simulations, we additionally perform a model-data comparison
23 using proxy-based temperature anomalies that are available for the northern high latitudes (CAPE Last
24 Interglacial Project Members, 2006), across the globe (Turney and Jones, 2010), and in middle to high
25 latitudes (Capron et al., 2014). The temperature reconstructions from CAPE Last Interglacial Project
26 Members (2006) are based on terrestrial and marine proxy records and estimate summer temperatures
27 for maximum LIG warmth relative to PI. The global dataset by Turney and Jones (2010) comprises
28 terrestrial and marine proxy records and estimates annual mean temperatures for maximum LIG
29 warmth (terrestrial) and for the period of plateaued $\delta^{18}\text{O}$ (marine), relative to present day (PD, 1961–

1 1990; Smith and Reynolds, 1998; New et al., 1999). The high latitude climate synthesis by Capron et
2 al. (2014) provides temporal air and sea surface temperature (SST) reconstructions based on ice core
3 and marine records respectively, across the interval 130 to 115 kyr BP (in our study covering the period
4 between 125 and 115 kyr BP). They also propose snapshots of surface temperature anomalies and
5 associated quantitative uncertainties at 115, 120, 125, and 130 kyr BP, but here we use the last two
6 snapshots. Detailed information regarding the proxy data is given in CAPE Last Interglacial Project
7 Members (2006), Turney and Jones (2010), and Capron et al. (2014), respectively.

8 In order to quantify the agreement between model and data, we calculate the root-mean-square
9 deviation (RMSD) which is a measure of the differences between an estimator (y_{model}) and estimated
10 parameter (y_{data}) (Gauss and Stewart, 1995; Mudelsee, 2010). RMSD is defined in Eq. (2):

$$11 \quad \text{RMSD} = \sqrt{\frac{1}{n} \sum_{i=1}^n (y_{\text{model}} - y_{\text{data}})^2} \quad (2)$$

12 where y_{model} is the simulated TS anomaly at the location of the proxy record, y_{data} indicates the
13 reconstructed TS anomaly, and n is the number of data samples.

14 **3. Results**

15 In the first part of this section, we present results from our LIG GIS sensitivity simulations, focusing on
16 TS anomalies. Afterwards, a short description of results from the transient simulations is presented,
17 followed by the model-data comparison and consideration of potential uncertainties in the data.

18 **3.1 Greenland Ice Sheet elevation and albedo influence on global surface** 19 **temperature**

20 **3.1.1 Annual mean anomalies**

21 Figure 2 presents the effect on the global TS of lowering the GIS by half its preindustrial elevation by
22 various methods. We observe the strongest warming over Greenland (of up to +12.5°C) in the LIG-
23 1300m-alb (Figs. 1c and 2c). Northern North America and the Arctic Ocean warm by up to +2°C in all
24 GIS sensitivity simulations. A pronounced warming is found over the southernmost Southern Ocean of
25 up to +4°C (Fig. 2a–c).

26 The highest global mean (Southern Hemisphere) TS anomaly is simulated in LIG-1300m-alb with
27 an average of $\Delta\text{TS} = +0.37^\circ\text{C}$ ($\Delta\text{TS} = +0.31^\circ\text{C}$) (Table 2). However, for the Northern Hemisphere, the
28 highest average TS anomaly of $\Delta\text{TS} = +0.47^\circ\text{C}$ is found in LIG- $\times 0.5$ (Table 2). Consequently, the exact

1 method of changing GIS configuration influences the hemispheric temperature anomalies.

2 The most affected areas by changes in GIS configuration are the northern high latitudes, which
3 experience a warming of $\Delta TS = +1.45^\circ\text{C}$ in LIG-1300m-alb, and $\Delta TS = +1.07^\circ\text{C}$ and $\Delta TS = +1.03^\circ\text{C}$
4 in LIG- $\times 0.5$ and LIG-1300m, respectively. This indicates that albedo plays a significant role in the
5 northern high latitude temperature changes, causing an average temperature anomaly of $\Delta TS =$
6 $+0.42^\circ\text{C}$. A local cooling of up to -1.60°C is limited to the Barents Sea in LIG- $\times 0.5$ and LIG-1300m
7 (Fig. 2a, b), south-west of Greenland in LIG-1300m (Fig. 2b), and a cooling of up to -2.30°C over the
8 Sea of Okhotsk (western Pacific Ocean) in LIG-1300m-alb caused by a reduction in albedo in the
9 prescribed ice-free areas (Fig. 2c, d). In the latter simulation, the Barents Sea cooling is counteracted by
10 a warming caused by changes in albedo (Fig. 2d).

11 At 130 kyr BP, the AMOC was reduced by 3.5 Sv as compared to the PI (Table 2). However, a
12 reduction in GIS partly counteracts the negative anomaly and leads to an increase in the AMOC of up
13 to 2.2 Sv relative to LIG-ctl (Table 2).

14 **3.1.2 Winter and summer mean anomalies**

15 The seasonal effect of a reduced GIS elevation is strongest during local winter in both hemispheres in
16 all GIS sensitivity simulations (Table 2). However, for simplicity we focus here only on the GIS
17 sensitivity simulation that includes changes in GIS elevation and corresponding changes in albedo
18 (LIG-1300m-alb, Fig. 3). In the Northern (Southern) Hemisphere, winter TS changes by $\Delta TS =$
19 $+0.57^\circ\text{C}$ ($\Delta TS = +0.39^\circ\text{C}$), with the northern high latitudes (60–90°N) experiencing the highest positive
20 anomalies of $\Delta TS = +2.08^\circ\text{C}$ (Fig. 3a, Table 2).

21 During summer, the TS anomaly is also positive but of lower magnitude, with an average of $\Delta TS =$
22 $+0.24^\circ\text{C}$ for Northern Hemisphere, Southern Hemisphere, and globally (Fig. 3b, Table 2). The northern
23 high latitudes warm during summer by $\Delta TS = +0.46^\circ\text{C}$, which is a modest change compared to winter
24 warming. Relatively strong cooling occurs over the Sea of Okhotsk and south-west of Greenland (Fig.
25 3), again with the strongest effect being present during winter.

26 **3.2 Combined effects of LIG forcings on global surface temperature**

27 The combined effects on TS of reducing the GIS by 1300 m, adjusting albedo, and applying
28 astronomical changes that represent an LIG climatic setting are presented in Fig. 4. Assuming linearity
29 of the different climatic drivers, we can additionally split the anomaly of PI and LIG-1300m-alb-CH₄
30 (equivalent to LIG-1300m-alb, but with a CH₄ concentration adjusted to PI simulation) into the isolated

1 contributions of changes in elevation and albedo and in astronomical forcing (calculated as the
2 difference between the anomaly of LIG-1300m-alb-CH₄ and PI, and the anomaly of LIG-1300m-alb
3 and LIG-ctl).

4 Considering the TS values from Table 2, we find that the magnitude of the astronomical forcing
5 influence is stronger than the effects of lowering the GIS and respective adjustment of the albedo in the
6 global average of annual mean TS, as well as the annual mean average over Northern Hemisphere (Fig.
7 4a). In the Southern Hemisphere, both forcings have equal contributions to changes in annual mean TS
8 (Fig. 4a). During winter, changes in GIS have the strongest influence globally and in the Northern
9 Hemisphere, while in the Southern Hemisphere changes in astronomical forcing are dominant (Fig. 4b).
10 During summer, there is an opposite pattern (Fig. 4c). The strongest combined effect of insolation and
11 changes in GIS and albedo occurs in the Northern Hemisphere during summer with an anomaly of ΔTS
12 = +2.51°C. Globally, the combined effect leads to a warming of $\Delta TS = +1.34^\circ\text{C}$ during summer. In the
13 Southern Hemisphere, the strongest combined effect is simulated during winter with $\Delta TS = +1.08^\circ\text{C}$.

14 The winter (local minimum TS) of the LIG is in general cooler than the PI at northern low to
15 middle latitudes, while at northern high latitudes and Southern Hemisphere winter is warmer (Fig. 4b).
16 If we separate the astronomical effect from the GIS lowering and albedo changes, we can attribute to
17 insolation a cooling of $\Delta TS = -0.52^\circ\text{C}$ in Northern Hemisphere, and a warming of $\Delta TS = +0.69^\circ\text{C}$ in
18 Southern Hemisphere.

19 Summer (local maximum TS) anomalies of the LIG with respect to PI are stronger than winter
20 anomalies in the Northern Hemisphere (Fig. 4c). Strongest continental summer TS anomalies are
21 located in the Northern Hemisphere (up to $\Delta TS = +16.7^\circ\text{C}$). Locations where the LIG is cooler than PI
22 are found at $\sim 10^\circ\text{N}$ over Africa and at $\sim 25^\circ\text{N}$ over India.

23 **3.3 Surface temperature evolution during the present and Last Interglacial**

24 In Figs. 5, S2, and S3, a comparison of transient TS derived from the five transient simulations (Table
25 1) is shown. The LIG transient simulations are important for determining when the maximum LIG
26 warmth occurred in dependence of the location as well as seasons. The TS evolution in the northern
27 high latitudes (60–90°N) is displayed in Fig. 5. All LIG (130–115 kyr BP) simulations (LIG-ctl-tr, LIG-
28 $\times 0.5$ -tr, LIG-1300m-alb-tr, and LIG-GHG-tr) indicate a similar annual mean trend, starting with a
29 plateau until mid-LIG (around 123 kyr BP) followed by a pronounced cooling trend (Fig. 5a). The LIG-
30 ctl-tr starts at a slightly higher TS than the LIG-GHG-tr, but although the trace gas concentrations are
31 mostly lower throughout the latter, the LIG-GHG-tr simulates higher TS throughout the LIG. This

1 indicates that changes in the vegetation which are simulated in the LIG-ctl-tr lead to a cooling in the
2 Northern Hemisphere, partly counteracting the warming induced by higher GHG concentrations. The
3 most extreme case is represented by LIG-1300m-alb-tr, which shows predominantly the highest TS
4 relative to TS of other LIG transient simulations. The Holocene (8–0 kyr BP) transient simulation
5 (HOL-tr) starts also with a warming until around mid-Holocene (6 kyr BP), followed by a cooling
6 trend.

7 During winter, all LIG simulations indicate a positive trend in the early LIG, with maximum TS at
8 around mid-LIG (Fig. 5b), followed by a strong cooling. The relative order of magnitudes of TS trends
9 during different simulations is the same as for annual mean TS, but with a relatively larger offset in
10 between simulations. Simulation HOL-tr shows a warming, followed by a cooling trend that starts at
11 mid-Holocene (Fig. 5b). Winter TS are characterized by stronger temporal variability than summer TS
12 (Fig. 5b, c). Summer TS in all LIG simulations indicate a slight warming trend until around 128 to 126
13 kyr BP, followed by a pronounced cooling. The offset between transient TS is smaller than for annual
14 mean and winter, but with the same order on the temperature scale. A dramatic cooling is also present
15 in the Holocene simulation starting at mid-Holocene (Fig. 5c). Furthermore, the timing of the
16 maximum LIG warmth does not occur simultaneously between the winter and summer seasons, the
17 winter season indicating a later peak than summer (Figs. 5, S2, and S3).

18 **3.4 Comparison of model results to temperature reconstructions**

19 Due to the large amount of simulated data, we display in the model-data comparison simulated LIG TS
20 derived from only one equilibrium simulation with changes in GIS, namely LIG-1300m-alb. For the
21 calculation of the maximum LIG warmth, we consider the corresponding transient simulation (LIG-
22 1300m-alb-tr). However, the comparison of the proxy-based temperatures with the other GIS
23 sensitivity simulations is considered in Table S1 in the Supplementary material, which gives the RMSD
24 values between temperature reconstructions and simulated TS extracted at the location of each given
25 proxy record and derived from simulations with different GIS boundary conditions. Furthermore, we
26 display also results from control simulation for 130 kyr BP (LIG-ctl) and the corresponding transient
27 simulation (LIG-ctl-tr) for maximum LIG warmth, in order to determine if and where GIS changes lead
28 to an increase in model-data agreement.

29 **3.4.1 Proxy-based summer temperature reconstructions**

30 Figures 6, 8a, and S4a present a model-data comparison that consider LIG terrestrial and marine proxy-
31 based summer temperature anomalies relative to PI derived by CAPE Last Interglacial Project

1 Members (2006). Simulated and reconstructed temperature anomalies agree reasonably well with
2 respect to the sign of the change, in the simulation with a reduction in GIS (LIG-1300m-alb, Fig. 6a)
3 and with preindustrial GIS configuration (LIG-ctl, Fig. 6c). The best agreement between model and
4 proxy reconstructions occurs over northern Asia and Europe. In the North Atlantic Ocean and the Arctic
5 Ocean, the model underestimates marine-based temperature reconstructions (Fig. 6a, c). However, a
6 reduction in GIS and albedo leads to slightly higher summer temperature anomalies at the location of
7 some marine proxies in the North Atlantic Ocean, partly reducing the model-data mismatch (Fig. 6a).
8 Over Greenland, the elevation changes lead to an overestimation of the reconstructed temperature
9 anomalies – proxy records show anomalies of +4 to +5°C, while the simulated TS anomalies are above
10 +7°C (Fig. 6a). However, in the LIG-ctl, there is an underestimation of the reconstructed temperatures
11 (Fig. 6c).

12 In the case of the terrestrial proxies, the temperature span covers +2 to +6°C, while the
13 corresponding simulated anomalies cover +1 to +11°C. In addition to the 130 kyr BP simulation (LIG-
14 1300m-alb), for each given core location we also consider TS anomalies relative to PI calculated at the
15 minimum and maximum LIG summer warmth as derived from the LIG-1300m-alb-tr (Fig. 8a). In
16 about half the cases (14 records out of 27), the error bars touch the 1 : 1 line, possibly indicating better
17 agreement than when compared to summer TS anomalies at 130 kyr BP (Fig. 8a). However, the number
18 of 13 unresolved records can be reduced to 11, when the terrestrial proxy-based temperature anomalies
19 are compared to the LIG-ctl-tr (Fig. S4a). Marine-based temperature anomalies and the corresponding
20 simulated anomalies (from LIG-1300m-alb) cover temperature spans of 0 to +3°C and of ~0 to +4°C,
21 respectively (Fig. 8a). Seven out of thirteen marine records cannot be reconciled with the simulations
22 when considering maximum and minimum summer TS anomalies during the LIG (Figs. 8a and S4a).
23 When the reconstructed data is compared to simulated annual mean TS anomalies at 130 kyr BP (Figs.
24 S5a, c and S6) and at annual mean minimum or maximum LIG warmth (Figs. S5b, d and S6), we find
25 an even higher discrepancy than when compared to the summer average, implying that the
26 reconstructed records are indeed biased towards summer.

27 The proxy dataset by CAPE Last Interglacial Project Members (2006) is considered to represent
28 summer temperatures at the maximum LIG warmth. Thus, we additionally include in the model-data
29 comparison the simulated maximum LIG warmth calculated from our transient LIG simulations (Fig.
30 6b, d). We find that the agreement between model and data increases in some cases. For the northern
31 North Atlantic Ocean, for example, marine records agree best with simulated TS anomalies at the

1 maximum LIG warmth (between 121.5 and 124.5 kyr BP, Fig. 9a) in the LIG-1300m-alb (Fig. 6b).
2 However, the RMSD between the simulated TS and reconstructed temperature anomalies reveals that
3 the best agreement occurs with TS anomalies at maximum LIG warmth in the LIG-ctl-tr (Table S1 in
4 Supplementary material). A reduction in GIS, thus, does not improve in general the model-data
5 agreement when the dataset by CAPE Last Interglacial Project Members (2006) is considered.
6 However, changes in GIS lead to high temperature anomalies during local winter (Fig. 3a), while
7 summer season is not strongly influenced (Fig. 3b). Therefore, in a comparison with proxy
8 reconstructions that represent summer temperature anomalies, changes in GIS do not have a significant
9 impact on model-data agreement.

10 **3.4.2 Proxy-based annual mean temperature reconstructions**

11 Both reconstructed (Turney and Jones, 2010) and simulated global annual mean temperature
12 anomalies indicate that the high latitudes experienced warmer temperatures during the LIG than in the
13 PI, with strongest anomalies being present in the northern high latitudes (Fig. 7). However, the model
14 underestimates the strong positive anomalies derived from proxy records, and in low and middle
15 latitudes the model cannot capture the magnitude of the cooling that the proxy records show (Figs. 7a,
16 c, 8b, and S4b).

17 Changes in GIS have no significant influence in low to middle latitudes but cause strong positive
18 anomalies in the northern high latitudes thus improving the model-data comparison (Fig. 7a, Table S2),
19 although the model still underestimates the proxy reconstructions. Terrestrial proxy records indicate
20 stronger anomalies with $\Delta TS = +2.21^{\circ}\text{C}$ (globally), $\Delta TS = +2.21^{\circ}\text{C}$ (Northern Hemisphere), and $\Delta TS =$
21 $+2.11^{\circ}\text{C}$ (Southern Hemisphere). The corresponding simulated anomalies indicate a global average of
22 $\Delta TS = +1.44^{\circ}\text{C}$, underestimating the records by $\sim 1^{\circ}\text{C}$. The Northern Hemisphere and Southern
23 Hemisphere average TS anomalies are $\Delta TS = +1.48^{\circ}\text{C}$ and $\Delta TS = +0.92^{\circ}\text{C}$, respectively. Marine
24 records capture lower anomalies than their terrestrial counterparts but still larger anomalies than the
25 corresponding simulated anomalies.

26 The majority of the terrestrial records shows a stronger signal than the simulated anomalies (Fig. 8b).
27 The temperature anomaly range in the terrestrial reconstructed data covers -5 to $+15^{\circ}\text{C}$, while the
28 model covers 0 to $+12^{\circ}\text{C}$. Out of 100 terrestrial records, 33 agree with the simulated TS anomalies
29 somewhere between the annual mean minimum and maximum LIG warmth derived from LIG-1300m-
30 alb-tr (Fig. 8b), and 19 records with simulates TS anomalies derived from LIG-ctl-tr (Fig S4b).

31 The reconstructed marine temperature anomalies cover a range of -6 to $+11^{\circ}\text{C}$ compared to 0 to

1 +3°C in the model, indicating pronounced underestimation of the marine proxy-based anomalies by the
2 model (Figs. 7a and 8b). When we consider both annual mean minimum and maximum LIG warmth,
3 the simulated TS span increases by $\sim 1^\circ\text{C}$ (-0.5 to $+3.5^\circ\text{C}$). Twenty records (out of 162) agree with the
4 model data somewhere between the minimum and maximum LIG warmth with respect to annual mean
5 derived from LIG-1300m-alb-tr, and 25 records when LIG-ctl-tr is considered (Fig. S4b).

6 The proxy records derived by Turney and Jones (2010) are considered to record an annual mean
7 temperature signal. Nevertheless, some records may be biased towards a specific season. Therefore, we
8 also consider the minimum winter and maximum summer TS during the LIG (Fig. 4c). Seasonality
9 increases the span of the vertical bars, providing the possibility of a better agreement with the
10 reconstructed temperature anomalies. The agreement between proxy records and model simulations
11 increases, with 51 (69) terrestrial and 53 (51) marine records being reconciled by considering
12 seasonality derived from LIG-1300m-alb-tr (LIG-ctl-tr) (Figs. 4c and S4c).

13 As already mentioned, the terrestrial proxy records by Turney and Jones (2010) are considered to
14 record annual mean temperature anomalies at the maximum LIG warmth. Therefore, we additionally
15 compare the terrestrial records with the simulated annual mean at the LIG thermal maximum (Fig. 7b,
16 d). Over Europe, the agreement between model and data is increased for those records that indicate a
17 warming, since the simulated anomalies derived from LIG-1300m-alb-tr indicate a warming at the
18 maximum LIG warmth, while presenting nearly no change at 130 kyr BP (Fig. 7a). A better agreement
19 is found also over northern Asia. According to Table S2, the terrestrial proxy-based temperature
20 anomalies indicate the best agreement with the simulated annual mean TS at the maximum LIG
21 warmth derived from the LIG-1300m-alb. The annual mean anomalies are influenced by winter
22 temperatures, the season during which GIS leads to strong positive anomalies. Therefore, a model-data
23 comparison with proxy reconstructions that represent an annual mean signal shows a better agreement
24 than when summer proxies are considered.

25 **3.4.3 Time resolved proxy-based summer temperature reconstructions**

26 For a more robust model-data comparison, we additionally compare our simulated TS to a compilation
27 of high-latitude LIG temperature anomalies derived from synchronized records representing 130 kyr
28 BP (Figs. 10 and S12, Capron et al., 2014). The synchronization is performed by aligning marine
29 sediment records onto the recent AICC2012 ice chronology (Capron et al., 2014 and references
30 therein). This method reduces the uncertainty in relative dating of the proxy reconstructions. The
31 marine records from the North Atlantic Ocean indicate mostly negative anomalies, while the model

1 simulates nearly no changes. As shown above, GIS reduction leads to a small increase in summer TS
2 anomalies, thus increasing the model-data disagreement (Figs. 10a and S12a). A warming in the
3 Southern Ocean is captured by both the model and proxies, though the model underestimates the
4 reconstructions. Reducing the GIS and albedo leads to an increase in local summer TS anomalies in the
5 Southern Ocean bringing the model and data in slightly closer agreement (Figs. 10b and S12b).

6 Considering Table S3, the reconstructed temperatures agree best with the simulated summer TS at
7 125 kyr BP in LIG-125k (Fig. S15), which considers a reduced GIS configuration (as in the LIG-
8 1300m-alb), both indicating a warming. However, this result is not conclusive with respect to the GIS
9 elevation, as a simulation with preindustrial GIS elevation has not been yet performed for this
10 particular time slice. For 130 kyr BP, the best agreement occurs for the LIG-ctl but for annual mean
11 rather than summer, since the model simulates an annual mean cooling in the North Atlantic Ocean
12 (Fig. S5c).

13 A model-data comparison of LIG temperature trends is also considered in our study (Figs. S13 and
14 S14). The proxy-based temperature trends by Capron et al. (2014) is compared to the temperature
15 evolution derived from our transient simulations (LIG-ctl-tr and LIG-1300m-alb-tr), between 125 and
16 115 kyr BP. An underestimation of the proxies by the model is again found, as well as an
17 overestimation depending on the locations (Figs. S13 and S14). Changes in GIS do not strongly
18 influence the results, with the exception of a few locations where such changes lead to a less
19 pronounced warming simulated in LIG-ctl-tr, thus reducing the mismatch.

20 **4. Discussion**

21 **4.1 Effects of insolation and Greenland Ice Sheet elevation on surface** 22 **temperature**

23 The main focus of our study is to quantify the possible contribution of reduced GIS elevation in
24 comparison with the contribution of insolation forcing to the climate of the LIG.

25 We can confirm the importance of insolation for the Northern Hemisphere, especially for the
26 northern middle to high latitudes (Figs. 4, 6, 7, 10). The belt of decreased TS, observed around 10°N
27 over Africa and 25°N over Arabian Peninsula and India (Figs. 4a, b and 7a), is related to increased
28 cloud cover (Fig. S9) and increased summer precipitation of up to +6 mm d⁻¹ (not shown). This effect
29 has been described by Herold and Lohmann (2009), who propose a mechanism for the temperature
30 anomalies that relies on changes in insolation in conjunction with increased cloud cover and increased

1 evaporative cooling.

2 In general, and independent of GIS elevation we observe an annual mean global warming of $\Delta T_S =$
3 $+0.44^\circ\text{C}$ in our LIG simulations relative to PI, hinting to positive feedbacks (such as sea ice-albedo)
4 that amplify the high latitude insolation signal (Fig. 4).

5 In Section 3.1.2, we have shown that the most pronounced impact of reduced GIS elevation (in
6 LIG-1300m-alb) occurs during local winter in both hemispheres (Fig. 3a). The winter warming of up to
7 $+3^\circ\text{C}$ over the Arctic Ocean may be linked to a decrease in sea ice and a delayed response to a warming
8 occurring in October (not shown), which is caused by positive sea-ice-albedo feedbacks. A decrease in
9 albedo over Greenland has the strongest influence during summer especially over the southernmost
10 region (Figs. 2d and 3b), caused by insolation absorption by the ice-free land surface. Furthermore, we
11 note cold annual mean anomalies in the Barents Sea (Fig. 2a, b) and Sea of Okhotsk (Fig. 2c) caused by
12 an increase in sea ice cover.

13 The change in the GIS elevation leads also to a relatively strong warming in the southern high
14 latitudes, mainly off the coast of Antarctica, with the strongest positive anomaly occurring during local
15 winter (Fig. 3a) that coincides with a heat flux transfer anomaly from the ocean to the atmosphere (not
16 shown). Increased ocean heat flux during winter leads to a warming of the atmosphere. The Antarctic
17 warming is most likely related to warmer deep water as well as subsurface warming poleward of 50°N
18 in the North and South Atlantic Ocean. The warming may be attributed to enhanced AMOC (Table 2),
19 which plays an important role in the exchange of heat between the hemispheres and between
20 atmosphere and ocean. Our results indicate a weaker AMOC during the LIG as compared to the PI of
21 up to 3.5 Sv, but changes in GIS lead to an increase of up to 2.2 Sv (Table 2). The simulated increase in
22 AMOC in the sensitivity simulations may be triggered by increased salinity of up to + 1 psu in the
23 northern North Atlantic Ocean. Increased salinity cannot be explained by changes in precipitation
24 minus evaporation, which show positive anomalies in this area (not shown). Another contributing
25 factor to the enhanced AMOC may be an increase in the atmospheric flow due to a reduction in GIS
26 elevation. The low pressure system over Greenland and the high pressure system above Europe become
27 more extreme, enhancing the north-eastward air circulation (Fig. 11). We find that the higher the sea
28 level pressure (SLP) anomaly (Fig. 11), the stronger the AMOC (Table 2). This change could also
29 explain the positive TS anomalies of up to $+1^\circ\text{C}$ in the northern North Atlantic Ocean, with more heat
30 being transported poleward from the low latitudes (Fig. 2a–c). However, convection cannot be the only
31 explanation for the southern high latitudes warmth, since the heat would be dispersed towards the

1 Southern Hemisphere. We however note a large scale warming in the subsurface of the Southern Ocean
2 which is probably caused by positive feedbacks. This warming may be related to changes in the water
3 stratification. We observe an invigorated vertical mixing in the northern North Atlantic Ocean and a
4 suppressed vertical mixing in the Southern Ocean (not shown), the latter causing the heat at subsurface
5 to be preserved. The Southern Ocean has a large heat capacity leading to a long memory of the system.
6 Lags of up to three months occur in the surface layer including sea ice (amplifying factor via positive
7 ice-albedo and ice-insulation feedbacks), while long-term lags occur in deeper levels below the summer
8 mixed layer that store seasonal thermal anomalies (Renssen et al., 2005).

9 In contrast to our results that show an increase in the AMOC relative to GIS elevation changes,
10 Otto-Bliesner et al. (2006) and Bakker et al. (2012) find a weakening of the AMOC. Bakker et al.
11 (2012) infer that the AMOC is weaker by up to 14 % in a regional study of LIG climate of the North
12 Atlantic Ocean, prescribing a reduction of GIS elevation (by 700 m) and extent (reducing the ice
13 volume by 30%). The weakening of the AMOC is caused by additional freshwater runoff resulting
14 from a melting GIS, a factor that is not considered in our study and that would probably cancel out or
15 reduce the effect of changes in the atmospheric transport on the AMOC. In the study by Bakker et al.
16 (2012), reducing GIS elevation and extent leads to changes in the atmospheric flow pattern and creates
17 a special pattern of surface pressure anomalies. In particular in the Norwegian Sea, Barents Sea, and
18 south-east of Greenland, the low pressure system is weaker inhibiting the overturning circulation.

19 The reduction of the GIS elevation and albedo alone leads in the study by Bakker et al. (2012) to a
20 local warming of up to +4°C in July, a substantially lower anomaly (factor of ~3) than simulated in our
21 model for local summer when reducing both GIS and albedo. However, when comparing their
22 simulated data to proxy-based temperature anomalies relative to PI (CAPE Last Interglacial Project
23 Members, 2006), Bakker et al. (2012) find an overestimation of the temperature reconstruction over
24 Greenland, and an underestimation at eastern Europe and Baffin Island – locations where we find a
25 similar temperature tendency (Fig. 6a).

26 Another climate model study that considers a reduction in GIS topography by various methods has
27 been performed by Merz et al. (2014). In their GIS sensitivity simulations, performed with the
28 Community Climate System Model version 4 (CCSM4), they find a rather mixed signal in temperature
29 anomalies over Greenland relative to the predominant warming found in our simulations with changes
30 in GIS. During local winter, their model simulates a warming of up to +5°C in central Greenland and a
31 cooling of up to -12°C in areas that become flat and ice-free. However, changes in topography of GIS

1 do not have a significant influence on climate in the surrounding areas in the study by Merz et al.
2 (2014). This may be caused by the fact that in their simulations SSTs are prescribed, while in our study
3 the atmosphere model is interactively coupled to an ocean general circulation model. However, in their
4 study the GIS is reconstructed by means of high resolution ice sheet models, while we consider a
5 relatively simplistic representation of the GIS. Differences are found also with respect to changes in
6 low-level winds. They find a rather local influence of the GIS changes and no major effect on the large-
7 scale atmospheric circulation. Our model simulates an enhancement of low-level winds around GIS and
8 on SLP (Fig. 11). As such, the methods of reducing GIS and the model used have a strong influence on
9 the local and large-scale climate. Note, however, that the aims of our study and the study by Merz et al.
10 (2014) are different, since the latter focuses on local effects above Greenland, while our main focus is
11 on the GIS effects on large-scale climate.

12 **4.2 Surface temperature evolution during the Last Interglacial and the** 13 **Holocene**

14 Although our results are not directly comparable to those derived by Bakker et al. (2013), who analyze
15 transient LIG January and July temperature anomalies (simulated by seven different models) with
16 respect to PI while we use transient absolute TS for coldest and warmest month, the pattern of the
17 temperature evolution remains the same. We observe similarities in middle latitudes and in winter
18 temperatures at high latitudes characterized by a large variability, and also note a clear cooling trend for
19 summer caused by a decrease in summer insolation. At northern high latitudes, Bakker et al. (2013)
20 find July maximum LIG warmth at 128.4–125.1 kyr BP, while in middle latitudes the maximum occurs
21 at 129.4–126.3 kyr BP. We also observe a warmest month maximum at around 128 kyr BP for high and
22 middle latitudes. A July maximum LIG warmth is found in the study by Loutre et al. (2014) at 128 kyr
23 BP. They find that the summer SST during the LIG is smaller in the model than in the reconstructed
24 temperatures, especially in the North Atlantic Ocean, but taking into account the evolution of the
25 Northern Hemisphere ice sheets reduces the disagreement between model and data.

26 During winter, our simulations produce a clear high latitude TS maximum around mid-LIG, while
27 the middle latitudes experience peak warmth around 121–117 kyr BP. Bakker et al. (2014) compare
28 transient LIG and Holocene (8–0 kyr BP) temperature trends simulated by different models (including
29 our COSMOS LIG-GHG-tr and HOL-tr simulations). They find negative warmest month temperature
30 trends for both LIG and Holocene in the Northern Hemisphere. Bakker et al. (2013) find a linear
31 relation between changes in insolation and temperatures for both summer and winter and for all

1 latitudes. There are however some exceptions. In northern high-latitudes, the winter temperature
2 changes result mainly from sea-ice related feedbacks and are described as highly model-dependent. In
3 southern middle to high latitudes, winter temperatures are strongly affected by changes in GHG
4 concentrations. Comparing all LIG transient simulations with the Holocene in the three considered
5 latitudinal bands, we observe that the Holocene experiences mostly lower TS than during the LIG, and
6 is characterized by smaller trends.

7 In our LIG transient simulations, we find that the differences in TS between the different model
8 simulations at the beginning of the LIG (130 kyr BP) are higher than during the late LIG (115 kyr BP),
9 indicating that the impact of a reduced GIS is stronger at the beginning of the LIG as compared to
10 glacial inception (GI, 115 kyr BP). By using different approaches to simulate the LIG evolution, we
11 offer a bandwidth of possible temperatures at each given time.

12 **4.3 Model-data comparison**

13 In combination with changes in the GIS elevation and lower albedo, the insolation effect leads to high
14 positive summer TS anomalies in the Northern Hemisphere (Figs. 4c and 6a). The pattern of these
15 changes is observed also in another model study of the LIG that includes a reduction in GIS elevation
16 of 500 m (Otto-Bliesner et al., 2006). The study shows that the June-July-August (JJA) temperature
17 anomaly with respect to PI is positive in the Northern Hemisphere, especially over the continents – yet,
18 the magnitude of these changes is smaller than in our study. In order to validate their results, Otto-
19 Bliesner et al. (2006) compare the simulated temperature anomalies to proxy-based temperature
20 anomalies by CAPE Last Interglacial Project Members (2006). Comparing our model results to the
21 same proxy compilation, we see most similarities in the local summer, although at some locations the
22 magnitude differs. Over Greenland, the warming reaches +5°C according to the proxy reconstructions,
23 while our results show a higher warming caused by the reduction of the GIS. However, the results from
24 Otto-Bliesner et al. (2006) indicate an underestimation. This suggests that the GIS elevation during the
25 LIG may have not been so drastically reduced as prescribed in our model setup, but was still reduced
26 by at least 500 m. This conclusion is supported by another model-data comparison study (Stone et al.,
27 2013) that uses the same data compilation (CAPE Last Interglacial Project Members, 2006). In their
28 simulation produced with an AOGCM, Stone et al. (2013) find a good agreement between model and
29 reconstruction as well, but cannot capture the reconstructed strong warming over Greenland, their
30 simulation indicating a warming of up to +3.5°C. They imply that the GIS was reduced in the LIG as
31 compared to PI, but not completely deglaciated – in the simulation with a completely removed GIS,

1 they find much stronger temperature anomalies over Greenland of up to +16°C, higher than in our
2 findings when GIS is reduced to half its present elevation (Fig. 2). A high overestimation of
3 reconstructed temperatures by the model is found also by Otto-Bliesner et al. (2006) for a deglaciated
4 Greenland, with summer temperature anomalies being higher than +10°C. Although in our simulations
5 we do not completely remove the ice sheet, we find strong TS anomalies of up to +11°C.

6 A warming as high as $+8 \pm 4^\circ\text{C}$ is proposed by NEEM Community members (2013) for the peak
7 LIG warmth at 126 kyr BP, based on North Greenland Eemian Ice Drilling (NEEM) ice core. They
8 propose that the northwest GIS is characterized only by a modest reduction of 400 ± 250 m between
9 128 and 122 kyr BP. In our study, we find at the location of the NEEM ice core an annual mean
10 warming of +9.6°C at 125 kyr BP at a GIS height of 553 m, a warming that is within the temperature
11 range proposed by NEEM Community Members (2013). Antarctic ice cores indicate positive
12 temperature anomalies of up to +3.5°C (Capron et al., 2014), suggesting stronger warming than the
13 simulated TS. However, a reduction in GIS reduces the model-data disagreement.

14 We go one step further and perform an additional model–data comparison with global coverage
15 (Turney and Jones, 2010). This proxy compilation is included in another model–data comparison study
16 for the LIG (Lunt et al., 2013), using a multi-model approach including the LIG-GHG. None of the
17 model simulations used in their study consider a reduction of the GIS elevation or albedo. Lunt et al.
18 (2013) find as well that the models fail to capture the magnitude of the temperature change suggested
19 by the proxy data. In their study, none of the simulations manage to capture a strong high latitude
20 annual mean warming indicated by the terrestrial proxy data. In fact, most of the models suggest a
21 slight cooling over Europe and northern Asia and only a slight warming over Greenland, at 130 kyr BP.
22 The LIG-1300m-alb indicates a relatively higher warming, reducing the disagreement between model
23 and data. Over Antarctica, the simulated and reconstructed temperature anomalies indicate a warming
24 of similar magnitude, in contrast to the simulations performed by Lunt et al. (2013), where most of the
25 models indicate a slight cooling. These results imply that a reduced GIS during the LIG improves the
26 model-data comparison. The RMSD values support this assumption (Table S2), although differences
27 between the considered cases (i.e. with or without a reduction in GIS) are relatively small – in the
28 calculation of the RMSD, all the proxy records by Turney and Jones (2010) are considered, including a
29 large number of records in the low latitudes where a change in GIS has no influence.

30 In all considered simulations, the model does not capture the magnitude of the SST anomalies
31 derived from marine records. Such underestimation of proxy data by the models is also found in model-

1 data comparison studies for the Holocene (Masson-Delmotte et al., 2006; Brewer et al., 2007;
2 Sundqvist et al., 2010; Zhang et al., 2010; O'ishi and Abe-Ouchi, 2011; Braconnot et al., 2012;
3 Lohmann et al., 2013; Bakker et al., 2014). Lohmann et al. (2013) show that the simulated SST trends
4 systematically underestimate the marine proxy-based temperature trends, and suggest that such
5 discrepancies can be caused either by too simplistic interpretations of the proxy data (including dating
6 uncertainties and seasonal biases) or by underestimated long-term feedbacks in climate models, a
7 feature which is probably also valid for the LIG. Such long-term feedbacks missing in our model is for
8 example the soil which has been recently implemented in COSMOS (Stärz et al., 2016). A coupled ice
9 sheet model is already implemented in the COSMOS (Barbi et al., 2014; Gierz et al., 2015), but is a
10 relatively new tool. We did not consider this in our simulations, although potential effects of the ice
11 sheets during the LIG exist (e.g. Sutter et al., 2015).

12 As shown above, the TS in low to middle latitudes experience mostly no change in our simulation, in
13 contrast to the proxy-based SST anomalies that indicate strong positive or negative temperature
14 changes. Our results partly contradict results from another early LIG (130 kyr BP) model simulation
15 (Otto-Bliesner et al., 2013). Their Community Climate System Model 3 (CCSM3) simulates mostly a
16 cooling in the ocean, with the exception of the North Atlantic Ocean south of Greenland, where the
17 anomalies have the same sign as proxy-based SSTs by Turney and Jones (2010). The terrestrial records
18 located in the high latitudes indicate however a better agreement with the LIG-1300m-alb. Even when
19 considering mid-LIG (125 kyr BP) in both studies (see Figs. S11 for our study), the terrestrial data can
20 be better reconciled with the simulation in which GIS elevation and albedo are reduced, especially over
21 Antarctica where Otto-Bliesner et al. (2013) find a cooling. Nevertheless, the difference between the
22 magnitude of change in model and reconstruction is still large. One contributing factor to warmer
23 temperatures in the high latitudes in our study may be (as also proposed by Otto-Bliesner et al., 2013)
24 the vegetation feedback, which is included in our simulations. Over Greenland, the CCSM3 model
25 underestimates the data, while our model simulations with reduced GIS capture an overestimation.
26 Otto-Bliesner et al. (2013) propose that the Greenland ice records may capture temperatures associated
27 with a reduction in GIS elevation. This suggests again that the LIG GIS was lower, but possibly not as
28 low as prescribed in our study. Otto-Bliesner et al. (2013) take into account also possible seasonal
29 biases considered by Lohmann et al. (2013), comparing the proxy data to simulated JJA temperature
30 anomalies for which they find the best fit, suggesting that the proxies record boreal summer
31 temperatures. In our study, however, we find the best overall fit for simulated annual mean rather than

1 summer TS (Figs. S11a and S12a) in all three cases: reduced GIS and albedo at 130 kyr BP (LIG-
2 1300m-alb, Figs. 7a and 8b) and at 125 kyr BP (LIG-125k, Figs. S11a, c), and preindustrial GIS at 130
3 kyr BP (LIG-ctl, Figs. 6c and S4b), with the best agreement between model and data in the first case
4 (Table S2). This could indicate that the proxies may indeed record annual mean temperatures, but in a
5 warmer climate caused by a reduced GIS (Fig. 7a). While the simulated summer TS are closer to the
6 proxies at some locations (e.g. Northern Asia and Europe, Figs. S7a, S8), there are still more records
7 that agree best with the simulated annual mean TS (Fig. 7a).

8 The proxy data compilation by Capron et al. (2014) used in our study is also compared to two
9 different climate models, namely CCSM3 and HadCM3. For 130 kyr BP, a model-data mismatch is
10 found in both cases, as most of the records indicate strong negative anomalies, while the models
11 simulate strong positive anomalies (Capron et al., 2014), especially CCSM3 which was run with higher
12 GHG concentrations than HadCM3 and COSMOS. With respect to the difference between model and
13 data, COSMOS simulates TS closer to the temperatures derived from marine-based records, since it
14 indicates nearly no change rather than a strong opposite signal. One cause for this modest change in the
15 North Atlantic Ocean may be related to vegetation changes, which may lead to a cooling as suggested
16 above. Another cause may be the decrease in AMOC at the LIG with respect to PI leading to the
17 bipolar seesaw, a pattern that is also observed in the proxy data at 130 kyr BP. We note a relative
18 cooling in both LIG simulations south of Iceland and Greenland. This region is very sensitive to
19 changes in the AMOC as shown in observational and numerical studies (Knight et al., 2005; Latif et al.,
20 2006; Dima and Lohmann, 2009).

21 For 125 kyr BP, COSMOS simulates higher anomalies in the North Atlantic Ocean than at 130 kyr
22 BP, but lower than CCSM3 and HadCM3 which simulate SSTs closer to the reconstructed
23 temperatures. Note however that the definition of summer is different in our study than in the study by
24 Capron et al. (2014), as they calculate it as the average of July-August-September, while we consider
25 the warmest month.

26 **4.4 Limitations of model-data comparison**

27 One challenge in an effective LIG model-data comparison is the difficulty to determine an absolute
28 dating of LIG marine paleo-proxy records (e.g. Drysdale et al., 2009), as few techniques exist for this
29 purpose. The dating of most of the records is derived by lining up their benthic $\delta^{18}\text{O}$ signal to a dated
30 benthic $\delta^{18}\text{O}$ stack (Lisiecki and Raymo, 2005). This strategy allows a relative dating of sediment cores
31 beyond the time limit of radiocarbon dating (Fairbanks et al., 2005; Chiu et al., 2007; Reimer et al.,

1 2009; Shanahan et al., 2012; Reimer et al., 2013), but it may lead to an artificial synchronization of all
2 records and therefore dampen regional differences in climate records with respect to the LIG
3 chronozone. An alternative method for synchronizing different types of proxies is used in Govin et al.
4 (2012), by aligning proxy records to the AICC2012 ice core chronology. Their study shows that the
5 maximum temperature changes during the LIG is different between the two hemispheres, the records
6 from Southern Ocean and Antarctica showing an early maximum compared to the records from
7 northern high latitudes. This method is used by Capron et al. (2014) in their proxy data compilation,
8 thus allowing for one less uncertainty in the model-data comparison. However, using such a time-
9 resolved temperature compilation does not improve our model-data comparison, as when compared to
10 the other proxy-based datasets that represent the maximum LIG warmth.

11 Additionally, some proxy records that are considered as recording annual mean temperatures are
12 seasonally biased, depending on the type of the proxy or on the region (Leduc et al., 2010; Schneider et
13 al., 2010; Lohmann et al., 2013). Furthermore, defining the timing of the maximum warmth during the
14 LIG represents as well a challenge. Bakker and Renssen (2014) show that the calculation of the
15 maximum LIG temperature is largely model-dependent, indicating also geographical- and time-
16 dependency (retrieved values differ between the annual mean and warmest month temperature
17 anomalies). They propose that the time-dependency originates from the dependency of the time
18 evolution of orbital forcing on latitude and seasons, as well as from the thermal inertia of the oceans
19 and from different feedbacks in the climate system. Our model results indicate that the timing of
20 maximum LIG warmth is indeed regionally dependent (Fig. 9).

21 **5. Conclusions**

22 In this study, we have analyzed data from several LIG sensitivity simulations performed with an
23 AOGCM and have assessed the influence of the GIS on global climate. We have compared the
24 simulated TS changes to anomalies as recorded by LIG climate data synthesis of CAPE Last
25 Interglacial Project Members (2006), Turney and Jones (2010), and of Capron et al. (2014).

26 We have shown that the exact method by which GIS configuration is changed has a significant
27 influence on hemispheric temperature anomalies. A reduction in GIS by 1300 m and changes in albedo
28 enhance the warming caused by changes in the astronomical forcing by up to +5°C. The LIG is much
29 warmer than the PI, especially during summer in the Northern Hemisphere, and during winter in the
30 Southern Hemisphere as well as northern high latitudes. The influence of astronomical forcing is
31 dominant (relative to changes in GIS) in the global and Northern Hemisphere average of annual mean

1 and local summer TS, and in the Southern Hemisphere winter. Changes in GIS have the strongest
2 influence (relative to insolation changes) globally and in the Northern Hemisphere winter average TS,
3 and in the Southern Hemisphere summer.

4 Modification of the GIS alone leads to a warming mostly in the northern and southern high latitudes.
5 Cooling occurs locally in Barents Sea or Sea of Okhotsk (depending on the simulation). The warming
6 caused by a reduced GIS has a winter rather than a summer signal at both hemispheres.

7 The simulated TS underestimate the temperature changes indicated by the proxy reconstructions.
8 However, a reduction in GIS elevation and extent improves the agreement between model and data by
9 Turney and Jones (2010). In order to obtain the maximum LIG warmth, we perform and analyze
10 transient model scenarios. For the proxy data by CAPE Last Interglacial Project Members (2006) that
11 represent summer temperatures, changes in GIS are of minor importance for SSTs.

12 Throughout the LIG, winter in the northern high latitudes is characterized by high temporal
13 variability, while summer TS indicate a clear cooling trend. By considering transient simulations with
14 different boundary conditions (i.e. GIS elevation, albedo, insolation, GHG concentrations) we offer a
15 bandwidth of potential temperatures at each given time throughout the LIG, between 130 and 115 kyr
16 BP. We reduce the mismatch between model and data by additionally considering uncertainties in
17 absolute dating of the proxy reconstructions, and uncertainties in the timing of maximum LIG warmth
18 (calculated in our study as the simulated maximum LIG warmth between 130 and 120 kyr BP at each
19 given location). The missing exact time constrain in CAPE Last Interglacial Project Members (2006)
20 and Turney and Jones (2010) provides therefore an additional uncertainty and complicates direct
21 model-data comparisons. Future studies that provide a better multi-proxy interpretation and a better
22 representation of the climate models are needed in order to reduce the model-data mismatch. Our
23 sensitivity simulations represent a starting point for future studies on transient integrations of the LIG
24 climate that include also transient changes in GIS elevation and extent, and for the comparison of such
25 results to high-quality proxy data. More sensitivity studies on the effects of a reduced GIS on global
26 climate are required in order to understand the response of different models to such changes, as the
27 ability of the models to properly simulate future states of the GIS is critical.

28

29 *Acknowledgement.* This study has been funded by the Deutsche Forschungsgemeinschaft (DFG) under
30 grant agreement no. LO 895/8-1 through priority programme INTERDYNAMIK (SPP 1266) and is
31 part of the project “Evaluation of Eemian and Holocene Climate Variability: Synthesis of marine

1 archives with climate modelling”. We are very grateful to an anonymous Referee and Emilie Capron
2 for the in-depth and helpful comments. Furthermore, we thank the many contributors for making the
3 temperature proxy-data available. We thank Dan Lunt for providing the formatted proxy-based dataset
4 of Turney and Jones (2010) and Emilie Capron for providing their temperature dataset.

5

6 **References**

- Alley, R. B., Andrews, J. T., Brigham-Grette, J., Clarke, G. K. C., Cuffey, K. M., Fitzpatrick, J. J., Funder, S., Marshall, S. J., Miller, G. H., Mitrovica, J. X., Muhs, D. R., Otto-Bliesner, B. L., Polyak, L., and White, J. W. C.: History of the Greenland Ice Sheet: paleoclimatic insights, *Quaternary Sci. Rev.*, 29, 1728–1756, doi:10.1016/S0277-3791(99)00062-1, 2010.
- Bakker, P. and Renssen, H.: Last Interglacial model–data mismatch of thermal maximum temperatures partially explained, *Clim. Past*, 9, 1633–1644, doi:10.5194/cpd-10-739-2014, 2014.
- Bakker, P., Van Meerbeeck, C. J., and Renssen, H.: Sensitivity of the North Atlantic climate to Greenland Ice Sheet melting during the Last Interglacial, *Clim. Past*, 8, 995–1009, doi:10.5194/cp-8-995-2012, 2012.
- Bakker, P., Stone, E. J., Charbit, S., Gröger, M., Krebs-Kanzow, U., Ritz, S. P., Varma, V., Khon, V., Lunt, D. J., Mikolajewicz, U., Prange, M., Renssen, H., Schneider, B., and Schulz, M.: Last interglacial temperature evolution – a model inter-comparison, *Clim. Past*, 9, 605–619, doi:10.5194/cp-9-605-2013, 2013.
- Bakker, P., Masson-Delmotte, V., Martrat, B., Charbit, S., Renssen, H., Gröger, M., Krebs-Kanzow, U., Lohman, G., Lunt, D. J., Pfeiffer, M., Phipps, S. J., Prange, M., Ritz, S. P., Schulz, M., Stenni, B., Stone, E. J., and Varma, V.: Temperature trends during the Present and Last Interglacial periods – a multi-model–data comparison, *Quaternary Sci. Rev.*, 99, 224–243, doi:10.1016/j.quascirev.2014.06.031, 2014.
- Barbi, D., Lohmann, G., Grosfeld, K., and Thoma, M.: Ice sheet dynamics within an Earth system model: coupling and first results on ice stability and ocean circulation, *Geosci. Model Dev.*, 7, 2003–2013, doi:10.5194/gmd-7-2003-2014, 2014.
- Bauch, H. A. and Erlenkeuser, H.: Interpreting glacial–interglacial changes in ice volume and climate from subarctic deep water foraminiferal $\delta^{18}\text{O}$, in: *Earth’s Climate and Orbital Eccentricity: The Marine Isotope Stage 11 Question*, edited by: Droxler, A. W., Poore, R. Z., and Burckle, L. H., American Geophysical Union Monograph Series, Washington DC, 87–102, doi:10.1029/137GM07, 2003.
- Berger, A. L.: Long-term variations of daily insolation and Quaternary climatic changes, *J. Atmos. Sci.*, 35, 2362–2367, doi:10.1175/1520-0469(1978)035<2362:LTVODI>2.0.CO;2, 1978.
- Berger, A. and Loutre, M. F.: Insolation values for the climate of the last 10 million years, *Quaternary Sci. Rev.*, 10, 297–317, doi:10.1016/0277-3791(91)90033-Q, 1991.
- Braconnot, P., Otto-Bliesner, B., Harrison, S., Joussaume, S., Peterchmitt, J.-Y., Abe-Ouchi, A., Crucifix, M., Driesschaert, E., Fichet, Th., Hewitt, C. D., Kageyama, M., Kitoh, A., Loutre,

- M.-F., Marti, O., Merkel, U., Ramstein, G., Valdes, P., Weber, L., Yu, Y., and Zhao, Y.: Results of PMIP2 coupled simulations of the Mid-Holocene and Last Glacial Maximum – Part 2: feedbacks with emphasis on the location of the ITCZ and mid- and high latitudes heat budget, *Clim. Past*, 3, 279–296, doi:10.5194/cp-3-279-2007, 2007.
- Braconnot, P., Harrison, S., Kageyama, M., Bartlein, P., Masson-Delmotte, V., Abe-Ouchi, A., Otto-Bliesner, B., and Zhao, Y.: Evaluation of climate models using palaeoclimatic data, *Nat. Clim. Change*, 2, 417–424, doi:10.1038/nclimate1456, 2012.
- Brewer, S., Guiot, J., and Torre, F.: Mid-Holocene climate change in Europe: a data-model comparison, *Clim. Past*, 3, 499–512, doi:10.5194/cp-3-499-2007, 2007.
- Brovkin, V., Raddatz, T., Reick, C. H., Claussen, M., and Gayler, V.: Global biogeophysical interactions between forest and climate, *Geophys. Res. Lett.*, 36, L07405, doi:10.1029/2009GL037543, 2009.
- CAPE-members – Anderson, P., Bennike, O., Bigelow, N., Brigham-Grette, J., Duvall, M., Edwards, M., Fréchette, B., Funder, S., Johnsen, S., Knies, J., Koerner, R., Lozhkin, A., MacDonald, G., Marshall, S., Matthiessen, J., Miller, G., Montoya, M., Muhs, D., Otto-Bliesner, B., Overpeck, J., Reeh, N., Sejrup, H. P., Turner, C., and Velichko, A.: Last Interglacial Arctic warmth confirms polar amplification of climate change, *Quaternary Sci. Rev.*, 25, 1383–1400, doi:10.1016/j.quascirev.2006.01.033, 2006.
- Capron, E., Govin, A., Stone, E. J., Masson-Delmotte, V., Mulitza, S., Otto-Bliesner, B. L., Rasmussen, T. L., Sime, L. C., Waelbroeck, C., and Wolff, E. W.: Temporal and spatial structure of multi-millennial temperature changes at high latitudes during the Last Interglacial, *Quaternary Sci. Rev.*, 103, 116–133, doi:10.1016/j.quascirev.2014.08.018, 2014.
- Carlson, A. E., Stoner, J. S., Donnelly, J. P., and Hillaire-Marcel, C.: Response of the southern Greenland Ice Sheet during the last two deglaciations, *Geology*, 36, 359–362, doi:10.1130/G24519A.1, 2008.
- Chiu, T.-C., Fairbanks, R. G., Cao, L., and Mortlock, R. A.: Analysis of the atmospheric ^{14}C record spanning the past 50,000 years derived from high-precision $^{230}\text{Th}/^{234}\text{U}/^{238}\text{U}$ and $^{231}\text{Pa}/^{235}\text{U}$ and ^{14}C dates on fossil corals, *Quaternary Sci. Rev.*, 26, 18–36, doi:10.1016/j.quascirev.2006.06.015, 2007.
- Church, J. A., Clark, P. U., Cazenave, A., Gregory, J. M., Jevrejeva, S., Levermann, A., Merrifield, M. A., Milne, G. A., Nerem, R. S., Nunn, P. D., Payne, A. J., Pfeffer, W. T., Stammer, D., and Unnikrishnan, A. S.: Sea level change, in: *Climate Change 2013: The Physical Science Basis, Contribution of Working Group I to the Fifth Assessment Report of the Intergovernmental Panel on Climate Change*, edited by: Stocker, T. F., Qin, D., Plattner, G.-K., Tignor, M., Allen, S. K., Boschung, J., Nauels, A., Xia, Y., Bex, V., and Midgley, P. M., Cambridge University Press, Cambridge, UK and New York, USA, 1137–1216, 2013.
- CLIMAP Project Members: The Last Interglacial ocean, *Quaternary Res.*, 21, 123–224, 1984.
- Collins, M., Knutti, R., Arblaster, J., Dufresne, J.-L., Fichet, T., Friedlingstein, P., Gao, X., Gurowki, W. J., Johns, T., Krinner, G., Shongwe, M., Tebaldi, C., Weaver, A. J., and Wehner, M.: Long-term climate change: projections, commitments and irreversibility, in: *Climate Change 2013: The Physical Science Basis, Contribution of Working Group I to the Fifth*

- Assessment Report of the Intergovernmental Panel on Climate Change, edited by: Stocker, T. F., Qin, D., Plattner, G.-K., Tignor, M., Allen, S. K., Boschung, J., Nauels, A., Xia, Y., Bex, V., and Midgley, P. M., Cambridge University Press, Cambridge, UK and New York, USA, 1029–1136, 2013.
- Colville, E. J., Carlson, A. E., Beard, B. L., Hatfield, R. G., Stoner, J. S., Reyes, A. V., and Ullman, D. J.: Sr-Nd-Pb isotope evidence for ice-sheet presence on southern Greenland during the last interglacial, *Science*, 333 (6042), 620–623, doi:10.1126/science.1204673, 2011.
- Crowley, T. J. and Kim, K.-Y.: Milankovitch forcing of the Last Interglacial sea level, *Science*, 265, 1566–1568, 1994.
- Cuffey, K. M. and Marshall, S. J.: Substantial contribution to sea-level rise during the last interglacial from the Greenland ice sheet, *Nature*, 404, 591–594, doi:10.1038/35007053, 2000.
- Dima, M. and Lohmann, G.: Evidence for Two Distinct Modes of Large-Scale Ocean Circulation Changes over the Last Century. *J. Climate*, 23, 5–16, doi:10.1175/2009JCLI2867.1, 2010.
- Dowsett, H. J., Foley, K. M., Stoll, D. K., Chandler, M. A., Sohl, L. E., Bentsen, M., Otto-Bliesner, B. L., Bragg, F. J., Chan, W.-L., Contoux, C., Dolan, A. M., Haywood, A. M., Jonas, J. A., Jost, A., Kamae, Y., Lohmann, G., Lunt, D. J., Nisancioglu, K. H., Abe-Ouchi, A., Ramstein, G., Riesselman, C. R., Robinson, M. M., Rosenbloom, N. A., Salzmann, U., Stepanek, C., Strother, S. L., Ueda, H., Yan, Q., and Zhang, Z.: Sea surface temperature of the mid-Piacenzian ocean: a data-model comparison, *Scientific Reports*, 3, 2013, doi:10.1038/srep02013, 2013.
- Drysdale, R. N., Hellstrom, J. C., Zanchetta, G., Fallick, A. E., Sánchez-Goñi, M. F., Couchoud, I., McDonald, J., Maas, R., Lohmann, G., and Isola, I.: Evidence for obliquity forcing of glacial Termination II, *Science*, 325, 1527–1531, doi:10.1126/science.1170371, 2009.
- Dutton, A. and Lambeck, K.: Ice volume and sea level during the last interglacial, *Science*, 337, 216–219, doi:10.1126/science.1205749, 2012.
- Dutton, A., Carlson, A., Milne, G., Long, A. J., Clark, P. U., DeConto, R., Horton, B. P., Rahmstorf, S., Raymo, M. E.: Sea-level rise due to polar ice-sheet mass loss during past warm periods, *Science*, 349 (6244), doi: 10.1126/science.aaa4019, 2015.
- Eugster, W., Rouse, W., Pielke Sr., R. A., McFadden, J. P., Baldocchi, D., Kittel, D., Chapin III, T. G. F., Liston, F. S., Vidale, G. E., Vaganov, P. L., and Chambers, E. S.: Land-atmosphere energy exchange in Arctic tundra and boreal forest: available data and feedbacks to climate, *Global Change Biol.*, 6, 84–115, doi:10.1046/j.1365-2486.2000.06015.x, 2000.
- Fairbanks, R. G., Mortlock, R. A., Chiu, T.-C., Cao, L., Kaplan, A., Guilderson, T. P., Fairbanks, T. W., Bloom, A. L., Grootes, P. M., and Nadeau, M.-J.: Radiocarbon calibration curve spanning 0 to 50,000 years BP based on paired $^{230}\text{Th}/^{234}\text{U}/^{238}\text{U}$ and ^{14}C dates on pristine corals, *Quaternary Sci. Rev.*, 24, 1781–1796, doi:10.1016/j.quascirev.2005.04.007, 2005.
- Felis, T., Lohmann, G., Kuhnert, H., Lorenz, S. J., Scholz, D., Pätzold, J., Al Rousan, S. A., and Al-Moghrabi, S. M.: Increased seasonality in Middle East temperatures during the last interglacial period, *Nature*, 429, 164–168, doi:10.1038/nature02546, 2004.

- Felis, T., Giry, C., Scholz, D., Lohmann, G., Pfeiffer, M., Pätzold, J., Kölling, M., and Scheffers, S. R.: Tropical Atlantic temperature seasonality at the end of the last interglacial, *Nature Comm.*, 6, 6159, doi:10.1038/ncomms7159, 2015.
- Fitzjarrald, D. R. and Moore, K. E.: Turbulent transport over tundra, *J. Geophys. Res.-Atmos.*, 97, 16717–16729, doi:10.1029/91JD01030, 1992.
- Flato, G., Marotzke, J., Abiodun, B., Braconnot, P., Chou, S. C., Collins, W., Cox, P., Driouech, F., Emori, S., Eyring, V., Forest, C., Gleckler, P., Guilyardi, E., Jakob, C., Kattsov, V., Reason, C., and Rummukainen, M.: Evaluation of climate models, in: *Climate Change 2013: The Physical Science Basis, Contribution of Working Group I to the Fifth Assessment Report of the Intergovernmental Panel on Climate Change*, edited by: Stocker, T. F., Qin, D., Plattner, G.-K., Tignor, M., Allen, S. K., Boschung, J., Nauels, A., Xia, Y., Bex, V., and Midgley, P. M., Cambridge University Press, Cambridge, UK and New York, USA, 741–866, 2013.
- Gauss, C. F. and Stewart, G. W.: *Theory of the Combination of Observations Least Subject to Error: Part One, Part Two, Supplement*, vol. 11, *Classics in Applied Mathematics*, Society for Industrial and Applied Mathematics, doi:10.1137/1.9781611971248, 1995.
- Gierz, P., Lohmann, G., and Wei, W.: Response of Atlantic Overturning to Future Warming in a coupled Atmosphere-Ocean-Ice Sheet Model, *Geophys. Res. Lett.*, 42, 6811–6818, doi:10.1002/2015GL065276, 2015.
- Gong, X., Knorr, G., Lohmann, G., and Zhang, X.: Dependence of abrupt Atlantic meridional ocean circulation changes on climate background states, *Geophys. Res. Lett.*, 40, 3698–3704, doi:10.1002/grl.50701, 2013.
- Gong, X., Zhang, X., Lohmann, G., Wei, W., Zhang, Xu, and Pfeiffer, M.: Higher Laurentide and Greenland ice sheets strengthen the North Atlantic ocean circulation, *Clim. Dynam.*, 1–12, doi:10.1007/s00382-015-2502-8, 2015.
- Govin, A., Braconnot, P., Capron, E., Cortijo, E., Duplessy, J.-C., Jansen, E., Labeyrie, L., Landais, A., Marti, O., Michel, E., Mosquet, E., Risebrobakken, B., Swingedouw, D., and Waelbroeck, C.: Persistent influence of ice sheet melting on high northern latitude climate during the early Last Interglacial, *Clim. Past*, 8, 483–507, doi:10.5194/cp-8-483-2012, 2012.
- Govin, A., Capron, E., Tzedakis, P. C., Verheyden, S., Ghaleb, B., Hillaire-Marcel, C., St-Onge, G., Stoner, J. S., Bassinot, F., Bazin, L., Blunier, T., Combourieu Nebout, N., El Quahabi, A., Genty, D., Gersonde, R., Jiminez-Amat, P., Landais, A., Martrat, B., Masson-Delmotte, V., Parrenin, F., Seidenkrantz, M. S., Veres, D., Waelbroeck, C., and Zahn, R.: Sequence of events from the onset to the demise of the Last Interglacial: evaluating strengths and limitations of chronologies used in climatic archives, *Quaternary Sci. Rev.*, 129, 1–36, doi:10.1016/j.quascirev.2015.09.018, 2015.
- Harrison, S. P., Kutzbach, J. E., Prentice, C. E., Behling, P. J., and Sykes, M. T.: The response of Northern Hemisphere extratropical climate and vegetation to orbitally induced changes in insolation during the last interglaciation, *Quaternary Res.*, 43, 174–184, doi:10.1006/qres.1995.1018, 1995.
- Herold, M. and Lohmann, G.: Eemian tropical and subtropical African moisture transport: an isotope modelling study, *Clim. Dynam.*, 33, 1075–1088, doi:10.1007/s00382-008-0515-2,

2009.

- Hibler, W.: Dynamic thermodynamic sea ice model, *J. Phys. Oceanogr.*, 9, 815–846, 1979.
- Jansen, E., Overpeck, J., Briffa, K. R., Duplessy, J.-C., Joos, F., Masson-Delmotte, V., Olago, D., Otto-Bliesner, B., Peltier, W. R., Rahmstorf, S., Ramesh, R., Raynaud, D., Rind, D., Solomina, O., Villalba, R., and Zhang, D.: Palaeoclimate, in: *Climate Change 2007: The Physical Science Basis, Contribution of Working Group I to the Fourth Assessment Report of the Intergovernmental Panel on Climate Change*, edited by: Solomon, S., Qin, D., Manning, M., Chen, Z., Marquis, M., Averyt, K. B., Tignor, M., and Miller, H. L., Cambridge University Press, Cambridge, UK and New York, USA, 433–497, 2007.
- Jennings, R., Singarayer, J., Stone, E. J., Krebs-Kanzow, U., Khon, V., Nisancioglu, K. H., Pfeiffer, M., Zhang, X., Parker, A. G., Parton, A., Groucutt, H. S., White, T. S., Drake, N. A., and Petraglia, M. D.: The greening of Arabia: multiple opportunities for human occupation of the Arabian Peninsula during the Late Pleistocene inferred from an ensemble of climate model simulations, *Quatern. Int.*, 1–19, doi:10.1016/j.quaint.2015.01.006, 2015.
- Johnsen, S. J. and Vinther, B. M.: Greenland stable isotopes, in: *Encyclopedia of Quaternary Science*, Elsevier, 1250–1258, doi:10.1016/B0-444-52747-8/00345-8, 2007.
- Johnsen, S. J., Dahl-Jensen, D., Gundestrup, N., Steffensen, J.-P., Clausen, H. B., Miller, H., Masson-Delmotte, V., Sveinbjornsdottir, A. E., and White, J.: Oxygen isotope and palaeotemperature records from six Greenland ice-core stations: Camp Century, Dye-3, GRIP, GISP2, Renland and NorthGRIP, *J. Quaternary Sci.*, 16, 299–307, doi:10.1002/jqs.622, 2001.
- Jungclauss, J. H., Keenlyside, N., Botzet, M., Haak, H., Luo, J. J., Latif, M., Marotzke, J., Mikolajewicz, U., and Roeckner, E.: Ocean circulation and tropical variability in the coupled model ECHAM5/MPI-OM, *J. Climate*, 19, 3952–3972, doi:10.1175/JCLI3827.1, 2006.
- Kaspar, F. and Cubasch, U.: Simulations of the Eemian interglacial and the subsequent glacial inception with a coupled ocean atmosphere general circulation model, in: *The Climate of Past Interglacials*, edited by: Sirocko, F., Litt, T., Claussen, M., and Sánchez-Goñi, M. F., Elsevier, *Developments in Quaternary Sciences*, 7, Chap. 33, 499–515, doi:10.1016/S1571-0866(07)80058-3, 2007.
- Kaspar, F., Kühl, N., Cubasch, U., and Litt, T.: A model–data comparison of European temperatures in the Eemian interglacial, *Geophys. Res. Lett.*, 32, L11703, doi:10.1029/2005GL022456, 2005.
- Kirtman, B., Power, S. B., Adedoyin, J. A., Boer, G. J., Bojariu, R., Camilloni, I., Doblus-Reyes, F. J., Fiore, A. M., Kimoto, M., Meehl, G. A., Prather, M., Sarr, A., Schär, C., Sutton, R., van Oldenborgh, G. J., Vecchi, G., and Wang, H. J.: Near-term climate change: projections and predictability, in: *Climate Change 2013: The Physical Science Basis. Contribution of Working Group I to the Fifth Assessment Report of the Intergovernmental Panel on Climate Change*, edited by: Stocker, T. F., Qin, D., Plattner, G.-K., Tignor, M., Allen, S. K., Boschung, J., Nauels, A., Xia, Y., Bex, V., and Midgley, P. M., Cambridge University Press, Cambridge, UK and New York, USA, 953–1028, 2013.
- Knight, R. A., Allan, R. J., Folland, C. K., Vellinga, M., and Mann, M. E. A.: A signature of persistent natural thermohaline circulation cycles in observed climate, *Geophys. Res. Lett.*,

- 32, L20708, doi:10.1029/2005GL024233, 2005.
- Knorr, G. and Lohmann, G.: A warming climate during the Antarctic ice sheet growth at the Middle Miocene transition, *Nat. Geosci.*, 7, 376–381, doi:10.1038/NGEO2119, 2014.
- Knorr, G., Butzin, M., Micheels, A., and Lohmann, G.: A warm Miocene climate at low atmospheric CO₂ levels, *Geophys. Res. Lett.*, 38, L20701, doi:10.1029/2011GL048873, 2011.
- Koerner, R. M.: Ice-core evidence for extensive melting of the Greenland Ice Sheet in the last interglacial, *Science*, 244, 964–968, 1989.
- Koerner, R. M. and Fisher, D. A.: Ice-core evidence for widespread Arctic glacier retreat in the last interglacial and the early Holocene, *Ann. Glaciol.*, 35, 19–24, doi:10.3189/172756402781817338, 2002.
- Kopp, R. E., Simons, F. J., Mitrovica, J. X., Maloof, A., and Oppenheimer, M.: Probabilistic assessment of sea level during the last interglacial stage, *Nature*, 462, 863–867, doi:10.1038/nature08686, 2009.
- Kopp, R. E., Simons, F. J., Mitrovica, J. X., Maloof, A., and Oppenheimer, M.: Probabilistic assessment of sea level variations within the last interglacial stage, *Geophys. J. Int.*, 193, 711–716, doi:10.1093/gji/ggt029, 2013.
- Kukla, G. J., Bender, M. L., de Beaulieu, J. L., Bond, G., Broecker, W. S., Cleveringa, P., Gavin, J. E., Herbert, T. D., Imbrie, J., Jouzel, J., Keigwin, L. D., Knudsen, K.-L., McManus, J. F., Merkt, J., Muhs, D. R., Müller, H., Poore, R. Z., Porter, S. C., Seret, G., Shackleton, N. J., Turner, C., Tzedakis, P. C., and Winograd, I. J.: Last interglacial climates, *Quaternary Res.*, 58, 2–13, doi:10.1006/qres.2001.2316, 2002.
- Kutzbach, J. E., Gallimore, R. G., and Guetter, P. J.: Sensitivity experiments on the effect of orbitally-caused insolation changes on the interglacial climate of high northern latitudes, *Quatern. Int.*, 10–12, 223–229, doi:10.1016/1040-6182(91)90054-R, 1991.
- Langebroek, P. M. and Nisancioglu, K. H.: Simulating last interglacial climate with NorESM: role of insolation and greenhouse gases in the timing of peak warmth, *Clim. Past*, 10, 1305–1318, doi:10.5194/cp-10-1305-2014, 2014.
- Laskar, J., Robutel, P., Joutel, F., Gastineau, M., Correia, A. C. M., and Levrard, B.: A long-term numerical solution for the insolation quantities of the Earth, *Astron. Astrophys.*, 428, 261–285, doi:10.1051/0004-6361:20041335, 2004.
- Latif, M., Boning, C., Willebrand, J., Biastoch, A., Dengg, J., Keenlyside, N., Schweckendiek, U., and Madec, G.: Is the thermohaline circulation changing?, *J. Climate*, 19, 4631–4637, doi:10.1175/JCLI3876.1, 2006.
- Leduc, G., Schneider, R. R., Kim, J. H., and Lohmann, G.: Holocene and Eemian sea surface temperature trends as revealed by alkenone and Mg/Ca paleothermometry, *Quaternary Sci. Rev.*, 29, 989–1004, doi:10.1016/j.quascirev.2010.01.004, 2010.
- Lhomme, N., Clarke, G. K. C., and Ritz, C.: (2005): Global budget of water isotopes inferred from polar ice sheets, *Geophys. Res. Lett.*, 32, L20502, doi:10.1029/2005GL023774, 2005.
- Lisiecki, L. E. and Raymo, M. E.: A Pliocene-Pleistocene stack of 57 globally distributed benthic

- $\delta^{18}\text{O}$ records, *Paleoceanography*, 20, PA1003, doi:10.1029/2004PA001071, 2005.
- Lohmann, G. and Lorenz, S. J.: Orbital forcing on atmospheric dynamics during the last interglacial and glacial inception, in: *The Climate of Past Interglacials*, edited by: Sirocko, F., Claussen, M., Sánchez-Goñi, M. F., and Litt, T., Elsevier, *Developments in Quaternary Science*, 7, 527–546, 2007.
- Lohmann, G., Pfeiffer, M., Laepple, T., Leduc, G., and Kim, J.-H.: A model–data comparison of the Holocene global sea surface temperature evolution, *Clim. Past*, 9, 1807–1839, doi:10.5194/cp-9-1807-2013, 2013.
- Lorenz, S. J. and Lohmann, G.: Acceleration technique for Milankovitch type forcing in a coupled atmosphere–ocean circulation model: method and application for the Holocene, *Clim. Dynam.*, 23, 727–743, doi:10.1007/s00382-004-0469-y, 2004.
- Loulergue, L., Schilt, A., Spahni, R., Masson-Delmotte, V., Blunier, T., Lemieux, B., Barnola, J.-M., Raynaud, D., Stocker, T. F., and Chappellaz, J.: Orbital and millennial-scale features of atmospheric CH_4 over the past 800,000 years, *Nature*, 453, 383–386, doi:10.1038/nature06950, 2008.
- Loutre, M. F., Fichet, T., Goosse, H., Huybrechts, P., Goelzer, H., and Capron, E.: Factors controlling the last interglacial climate as simulated by LOVECLIM1.3, *Climate of the Past*, 10, 1541–1565, doi:10.5194/cp-10-1541-2014, 2014.
- Lüthi, D., Le Floch, M., Bereiter, B., Blunier, T., Barola, J. M., Siegenthaler, U., Raynaud, D., Jouzel, J., Fischer, H., Kawamura, K., and Stocker, T. F.: High-resolution carbon dioxide concentration record 650,00–800,000 years before present, *Nature*, 453, 379–382, doi:10.1038/nature06949, 2008.
- Lunt, D. J., Abe-Ouchi, A., Bakker, P., Berger, A., Braconnot, P., Charbit, S., Fischer, N., Herold, N., Jungclauss, J. H., Khon, V. C., Krebs-Kanzow, U., Langebroek, P. M., Lohmann, G., Nisancioglu, K. H., Otto-Bliesner, B. L., Park, W., Pfeiffer, M., Phipps, S. J., Prange, M., Rachmayani, R., Renssen, H., Rosenbloom, N., Schneider, B., Stone, E. J., Takahashi, K., Wei, W., Yin, Q., and Zhang, Z. S.: A multi-model assessment of last interglacial temperatures, *Clim. Past*, 9, 699–717, doi:10.5194/cp-9-699-2013, 2013.
- Marsland, S. J., Haak, H., Jungclauss, J. H., Latif, M., and Röske, F.: The Max-Planck-Institute global ocean/sea ice model with orthogonal curvilinear coordinates, *Ocean Model.*, 5, 91–127, doi:10.1016/S1463-5003(02)00015-X, 2003.
- Masson-Delmotte, V., Kageyama, M., Braconnot, P., Charbit, S., Krinner, G., Ritz, C., Guilyardi, E., Jouzel, J., Abe-Ouchi, A., Crucifix, M., Gladstone, R. M., Hewitt, C. D., Kitoh, A., LeGrande, A. N., Marti, O., Merkel, U., Motoi, T., Ohgaito, R., Otto-Bliesner, B., Peltier, W. R., Ross, I., Valdes, P. J., Vettoretti, G., Weber, S. L., Wolk, F., and Yu, Y.: Past and future polar amplification of climate change: climate model intercomparisons and ice-core constraints, *Clim. Dynam.*, 26, 513–529, doi:10.1007/s00382-005-0081-9, 2006.
- Masson-Delmotte, V., Schulz, M., Abe-Ouchi, A., Beer, J., Ganopolski, A., González Rouco, J. F., Jansen, E., Lambeck, K., Luterbacher, J., Naish, T., Osborn, T., Otto-Bliesner, B., Quinn, T., Ramesh, R., Rojas, M., Shao, X., and Timmermann, A.: Information from Paleoclimate archives, in: *Climate Change 2013: The Physical Science Basis, Contribution of Working*

- Group I to the Fifth Assessment Report of the Intergovernmental Panel on Climate Change, edited by: Stocker, T. F., Qin, D., Plattner, G.-K., Tignor, M., Allen, S. K., Boschung, J., Nauels, A., Xia, Y., Bex, V., and Midgley, P. M., Cambridge University Press, Cambridge, UK and New York, USA, 383–464, 2013.
- McKay, N. P., Overpeck, J. T., and Otto-Bliesner, B. L.: The role of ocean thermal expansion in Last Interglacial sea level rise, *Geophys. Res. Lett.*, 38, L14605, doi:10.1029/2011GL048280, 2011.
- Mearns, L. O., Hulme, M., Carter, T. R., Leemans, R., Lal, M., and Whetton, P.: Climate scenario development, in: *Climate Change 2001: The Scientific Basis, Contribution of Working Group I to the Third Assessment Report of the Intergovernmental Panel on Climate Change*, edited by: Houghton, J. T., Ding, Y., Griggs, D. J., Noguer, M., van der Linden, P. J., Dai, X., Maskell, K., and Johnson, C. A., Cambridge University Press, Cambridge, UK and New York, USA, 739–768, 2001.
- Merz, N., Born, A., Raible, C. C., Fischer, H., and Stocker, T. F.: Dependence of Eemian Greenland temperature reconstructions on the ice sheet topography, *Clim. Past*, 10, 1221–1238, doi:10.5194/cp-10-1221-2014, 2014.
- Montoya, M., von Storch, H., and Crowley, T. J.: Climate simulation for 125 kyr BP with a coupled ocean–atmosphere general circulation model, *J. Climate*, 13, 1057–1071, doi:10.1175/1520-0442(2000)013<1057:CSFKBW>2.0.CO;2, 2000.
- Mudelsee, M.: *Climate Time Series Analysis, Classical Statistical and Bootstrap Methods*, Atmospheric and Oceanographic Sciences Library, vol. 42, Springer, Dordrecht, 2010.
- NEEM community members: Eemian interglacial reconstructed from a Greenland folded ice core, *Nature*, 493, 498–494, doi:10.1038/nature11789, 2013.
- New, M., Hulme, M., and Jones, P.: Representing twentieth-century space–time climate variability, Part I: Development of a 1961–90 mean monthly terrestrial climatology, *J. Climate*, 12, 829–856, doi:10.1175/1520-0442(1999)012<0829:RTCSTC>2.0.CO;2, 1999.
- North Greenland Ice Core Project members: High-resolution record of Northern Hemisphere climate extending into the last interglacial period, *Nature*, 431, 147–151, doi:10.1038/nature02805, 2004.
- O’ishi, R. and Abe-Ouchi, A.: Polar amplification in the mid-Holocene derived from dynamical vegetation change with a GCM, *Geophys. Res. Lett.*, 38, L14702, doi:10.1029/2011GL048001, 2011.
- Otto-Bliesner, B. L., Marshall, S. J., Overpeck, J. T., Miller, G. H., Hu, A., and CAPE Last Interglacial Project members: simulating Arctic Climate Warmth and Icefield Retreat in the Last Interglaciation, *Science*, 311, 1751–1753, doi:10.1126/science.1120808, 2006.
- Otto-Bliesner, B. L., Rosenbloom, N., Stone, E. J., McKay, N. P., Lunt, D. J., Brady, E. C., and Overpeck, J. T.: How warm was the last interglacial? New model – data comparisons, *Philos. T. R. Soc. A*, 371, 1–20, doi:10.1098/rsta.2013.0097, 2013.
- Overpeck, J. T., Otto-Bliesner, B. L., Miller, G. H., Muhs, D. R., Alley, R. B., and Kiehl, J. T.: Paleoclimatic evidence for future ice-sheet instability and rapid sea-level rise, *Science*, 311,

1747–1750, doi:10.1126/science.1115159, 2006.

- Pfeiffer, M. and Lohmann, G.: The Last Interglacial as simulated by an Atmosphere-Ocean General Circulation Model: sensitivity studies on the influence of the Greenland Ice Sheet, in: *Earth System Science: bridging the Gaps between Disciplines Perspectives from a Multi-disciplinary Helmholtz Research School*, edited by: Lohmann, G., Grosfeld, K., Wolf-Gladrow, D., Unnithan, V., Notholt, J., and Wegner, A., Series: SpringerBriefs in Earth System Sciences, 57–64, Springer, Heidelberg, doi:10.1007/978-3-642-32235-8, 2013.
- Quiquet, A., Ritz, C., Punge, H. J., and Salas y Méliá, D.: Greenland ice sheet contribution to sea level rise during the last interglacial period: a modelling study driven and constrained by ice core data, *Clim. Past*, 9, 353–366, doi:10.5194/cp-9-353-2013, 2013.
- Raddatz, T. J., Reick, C. H., Knorr, W., Kattge, J., Roeckner, E., Schnur, R., Schnitzler, K. G., Wetzel, P., and Jungclaus, J.: Will the tropical land biosphere dominate the climate-carbon cycle feedback during the twenty-first century?, *Clim. Dynam.*, 29, 565–574, doi:10.1007/s00382-007-0247-8, 2007.
- Reimer, P. J., Baillie, M. G. L., Bard, E., Bayliss, A., Beck, J. W., Blackwell, P. G., Bronk Ramsey, C., Buck, C. E., Burr, G. S., Edwards, R. L., Friedrich, M., Grootes, P. M., Guilderson, T. P., Hajdas, I., Heaton, T. J., Hogg, A. G., Hughen, K. A., Kaiser, K. F., Kromer, B., McCormac, F. G., Manning, S. W., Reimer, R. W., Richards, D. A., Southon, J. R., Talamo, S., Turney, C. S. M., van der Plicht, J., and Weyhenmeyer, C. E.: IntCal09 and Marine09 radiocarbon age calibration curves, 0–50,000 years cal BP, *Radiocarbon*, 51, 1111–1150, 2009.
- Reimer, P. J., Bard, E., Bayliss, A., Beck, J. W., Blackwell, P. G., Bronk Ramsey, C., Buck, C. E., Cheng, H., Edwards, R. L., Friedrich, M., Grootes, P. M., Guilderson, T. P., Haflidason, H., Hajdas, I., Hatté, C., Heaton, T. J., Hoffmann, D. L., Hogg, A. G., Hughen, K. A., Kaiser, K. F., Kromer, B., Manning, S. W., Niu, M., Reimer, R. W., Richards, D. A., Scott, E. M., Southon, J. R., Staff, R. A., Turney, C. S. M., and van der Plicht, J.: IntCal13 and Marine13 radiocarbon age calibration curves 0–50,000 years cal BP, *Radiocarbon*, 55, 1869–1887, doi:10.2458/azu_js_rc.55.16947, 2013.
- Renssen, H., Goosse, H., Fichet, T., Masson-Delmotte, V., and Koç, N.: The Holocene climate evolution in the high-latitude Southern Hemisphere simulated by a coupled atmosphere-sea ice-ocean-vegetation model, *Holocene*, 15, 951–964, doi:10.1191/0959683605hl869ra, 2005.
- Robinson, A., Calov, R., and Ganopolski, A.: Greenland ice sheet model parameters constrained using simulations of the Eemian Interglacial, *Clim. Past*, 7, 381–396, doi:10.5194/cp-7-381-2011, 2011.
- Roeckner, E., Bäuml, G., Bonaventura, L., Brokopf, R., Esch, M., Giorgetta, M., Hagemann, S., Kirchner, I., Kornbluh, L., Manzini, E., Rhodin, A., Schlese, U., Schulzweida, U., and Tompkins, A.: The atmospheric general circulation model ECHAM5, Part I: Model description, Tech. Rep. 349, Max Planck Institute for Meteorology, Hamburg, Germany, 2003.
- Schneider, B., Leduc, G., and Park, W.: Disentangling seasonal signals in Holocene climate trends by satellite-model-proxy integration, *Paleoceanography*, 25, PA4217, doi:10.1029/2009PA001893, 2010.

- Semtner, A. J.: A model for the thermodynamic growth of sea ice in numerical investigations of climate, *J. Phys. Oceanogr.*, 6, 379–389, 1976.
- Shanahan, T. M., Beck, J. W., Overpeck, J. T., McKay, N. P., Pigati, J. S., Peck, J. A., Scholz, C. A., Heil Jr., C. W., and King, J.: Late Quaternary sedimentological and climate changes at Lake Bosumtwi Ghana: new constraints from laminae analysis and radiocarbon age modeling, *Palaeogeogr. Palaeoclimatol.*, 361–362, 49–60, doi:10.1016/j.palaeo.2012.08.001, 2012.
- Smith, T. M. and Reynolds, R. W.: A high-resolution global sea surface temperature climatology for the 1961–90 base period, *J. Climate*, 11, 3320–3323, doi:10.1175/1520-0442(1998)011<3320:AHRGSS>2.0.CO;2, 1998.
- Spahni, R., Chappellaz, J., Stocker, T. F., Loulergue, L., Hausammann, G., Kawamura, K., Fluckiger, J., Schwander, J., Raynaud, D., Masson-Delmotte, V., and Jouzel, J.: Atmospheric methane and nitrous oxide of the late Pleistocene from Antarctic ice cores, *Science*, 310, 1317–1321, doi:10.1126/science.1120132, 2005.
- Stärz, M., Lohmann, G., and Knorr, G.: The effect of a dynamic soil scheme on the climate of the mid-Holocene and the Last Glacial Maximum, *Clim. Past*, 12, 151–170, doi:10.5194/cp-12-151-2016, 2016.
- Stepanek, C. and Lohmann, G.: Modelling mid-Pliocene climate with COSMOS, *Geosci. Model Dev.*, 5, 1221–1243, doi:10.5194/gmd-5-1221-2012, 2012.
- Stirling, C. H., Esat, T. M., Lambeck, K., and McCulloch, M. T.: Timing and duration of the last interglacial: evidence for a restricted interval of widespread coral reef growth, *Earth Planet. Sc. Lett.*, 160, 745–762, doi:10.1016/S0012-821X(98)00125-3, 1998.
- Stone, E. J., Lunt, D. J., Annan, J. D., and Hargreaves, J. C.: Quantification of the Greenland ice sheet contribution to Last Interglacial sea level rise, *Clim. Past*, 9, 621–639, doi:10.5194/cp-9-621-2013, 2013.
- Sundqvist, H. S., Zhang, Q., Moberg, A., Holmgren, K., Körnich, H., Nilsson, J., and Brattström, G.: Climate change between the mid and late Holocene in northern high latitudes – Part 1: Survey of temperature and precipitation proxy data, *Clim. Past*, 6, 591–608, doi:10.5194/cp-6-591-2010, 2010.
- Sutter, J., Gierz, P., Grosfeld, K., Thoma, M., and Lohmann, G.: Ocean temperature thresholds for Last Interglacial West Antarctic Ice Sheet collapse, *Geophys. Res. Lett.*, doi:10.1002/2016GL067818, 2016, (in press).
- Tarasov, L. and W. R. Peltier: Greenland glacial history, borehole constraints, and Eemian extent, *J. Geophys. Res.*, 108(B3), 2143, doi:10.1029/2001JB001731, 2003.
- Turney, C. S. M. and Jones, R. T.: Does the Agulhas current amplify global temperatures during super-interglacials?, *J. Quaternary Sci.*, 25, 839–843, doi:10.1002/Jqs.1423, 2010.
- Valcke, S.: The OASIS3 coupler: a European climate modelling community software, *Geosci. Model Dev.*, 6, 373–388, doi:10.5194/gmd-6-373-2013, 2013.
- Valcke, S., Caubel, A., Declat, D., and Terray, L.: OASIS Ocean Atmosphere Sea Ice Soil users guide, Tech. Rep. TR/CMGC/03-69, CERFACS, Toulouse, France, 2003.

- van de Berg, W. J., van den Broeke, M., Ettema, J., van Meijgaard, E., and Kaspar, F.: Significant contribution of insolation to Eemian melting of the Greenland ice sheet, *Nat. Geosci.*, 4, 679–683, doi:10.1038/ngeo1245, 2011.
- Veeh, H. H.: $\text{Th}^{230}/\text{U}^{238}$ and $\text{U}^{234}/\text{U}^{238}$ ages of Pleistocene high sea level stand, *J. Geophys. Res.*, 71, 3379–3386, 1966.
- von Storch, H. and Zwiers, F. W.: *Statistical Analysis in Climate Research*, Cambridge University Press, New York, 1999.
- Wei, W. and Lohmann, G.: Simulated Atlantic Multidecadal Oscillation during the Holocene, *J. Climate*, 25, 6989–7002, doi:10.1175/JCLI-D-11-00667.1, 2012.
- Wei, W., Lohmann, G., and Dima, M.: Distinct modes of internal variability in the global meridional overturning circulation associated with the SH westerly winds, *J. Phys. Oceanogr.*, 42, 785–801, doi:10.1175/JPO-D-11-038.1, 2012.
- Willerslev, E., Cappellini, E., Boomsma, W., Nielsen, R., Hebsgaard, M. B., Brand, T. B., Hofreiter, M., Bunce, M., Poinar, H. N., Dahl-Jensen, D., Johnsen, S., Steffensen, J. P., Bennike, O., Schwenninger, J.-L., Nathan, R., Armitage, S., de Hoog, C.-J., Alfimov, V., Christl, M., Beer, J., Muscheler, R., Barker, J., Sharp, M., Penkman, K. E. H., Haile, J., Taberlet, P., Gilbert, M. T. P., Casoli, A., Campani, E., and Collins, M. J.: Ancient bio-molecules from deep ice cores reveal a forested southern Greenland, *Science*, 317, 111–114, doi:10.1126/science.1141758, 2007.
- Yin, Q. Z. and Berger, A.: Insolation and CO_2 contribution to the interglacial climate before and after the Mid-Brunhes Event, *Nat. Geosci.*, 3, 243–246, doi:10.1038/ngeo771, 2010.
- Zhang, Q., Sundqvist, H. S., Moberg, A., Körnich, H., Nilsson, J., and Holmgren, K.: Climate change between the mid and late Holocene in northern high latitudes – Part 2: Model-data comparisons, *Clim. Past*, 6, 609–626, doi:10.5194/cp-6-609-2010, 2010.
- Zhang, X., Lohmann, G., Knorr, G., and Xu, X.: Different ocean states and transient characteristics in Last Glacial Maximum simulations and implications for deglaciation, *Clim. Past*, 9, 2319–2333, doi:10.5194/cp-9-2319-2013, 2013.
- Zhang, X., Lohmann, G., Knorr, G., and Purcell, C.: Control of rapid glacial climate shifts by variations in intermediate ice-sheet volume, *Nature*, 512, 290–294, doi:10.1038/nature13592, 2014.

1 **Table and Figure captions**

2

3 **Table 1.** Overview of model configuration and climate forcings. PI = preindustrial, Veg. = vegetation;
4 dyn. = dynamic; e = eccentricity; ϵ = obliquity; ω = length of perihelion. The Greenland Ice Sheet
5 (GIS) configurations are displayed in Fig. 1. * Simulations presented in the supplementary material.

6

7 **Table 2.** Atlantic Meridional Overturning Circulation (AMOC) and absolute values of surface
8 temperature (TS) for global, Northern Hemisphere (NH), and Southern Hemisphere (SH) coverage,
9 calculated for annual mean, local summer mean (warmest month), and local winter mean (coldest
10 month).

11

12 **Figure 1.** Greenland Ice Sheet (GIS) elevation and land ice cover prescribed in our model simulations:
13 **(a)** preindustrial GIS and land ice mask, **(b)** $\times 0.5$ GIS and preindustrial land ice mask, **(c)** -1300 m GIS
14 and preindustrial land ice mask, **(d)** -1300 m and adjusted land ice mask. In **(a)**, the preindustrial
15 elevation and land ice mask are unchanged. In **(b)**, the preindustrial elevation over the GIS area is
16 multiplied by 0.5; the land ice mask is unchanged. In **(c)**, for each grid point over the GIS, 1300 m are
17 subtracted from preindustrial elevation; the land ice mask is unchanged. In **(d)**, for each grid point over
18 the GIS, 1300 m are subtracted from preindustrial elevation; at grid locations where the elevation is
19 lower than 1300 m, land ice is removed and albedo is adjusted accordingly.

20

21 **Figure 2.** Effect of **(a–c)** Greenland Ice Sheet elevation and **(c, d)** albedo in the 130 kyr BP
22 simulations. Annual mean surface temperature (TS) anomalies for: **(a)** LIG- $\times 0.5$ minus LIG-ctl, **(b)**
23 LIG-1300m minus LIG-ctl, **(c)** LIG-1300m-alb minus LIG-ctl, and **(d)** LIG-1300m-alb minus LIG-
24 1300m. Hatched areas mark statistically insignificant TS anomalies.

25

26 **Figure 3.** Effect of Greenland Ice Sheet elevation and albedo on surface temperature in the 130 kyr BP
27 simulation (LIG-1300m-alb). Same as Fig. 2c but for: **(a)** local winter mean (coldest month) and **(b)**
28 local summer mean (warmest month). Violet dashed lines represent the LIG-1300m-alb 50 %-
29 compactness sea ice isoline, violet continuous lines represent the LIG-1300m-alb sea ice edge. Green
30 dashed lines represent the LIG-ctl 50 %-compactness sea ice isoline, green continuous lines represent
31 the LIG-ctl sea ice edge.

1
2
3
4
5
6
7
8
9
10
11
12
13
14
15
16
17
18
19
20
21
22
23
24
25
26
27
28
29
30
31

Figure 4. Effect of Greenland Ice Sheet elevation, insolation, and albedo at 130 kyr BP relative to preindustrial (PI). Surface temperature (TS) anomalies between LIG-1300m-alb-CH₄ and PI for: **(a)** annual mean, **(b)** local winter mean (coldest month), and **(c)** local summer mean (warmest month). Violet dashed lines represent the LIG 50 %-compactness sea ice isoline, violet continuous lines represent the LIG sea ice edge. Green dashed lines represent the PI 50 %-compactness sea ice isoline, green continuous lines represent the PI sea ice edge. Hatched areas mark statistically insignificant TS anomalies.

Figure 5. Simulated surface temperature evolution for the Last Interglacial (LIG-) and the Holocene (8–0 kyr BP, HOL-tr) in northern high latitudes (60–90°N) calculated as running average with a window length of 21 model years representing 210 calendar years for: **(a)** annual mean, **(b)** local winter mean (coldest month), and **(c)** local summer mean (warmest month). The lower *x* scale represents the LIG time scale, the upper *x* scale indicates the Holocene time scale. The upper *x* scale is matched to the time scale between 128 and 120 kyr BP, assuming that Termination I and Termination II are similar with respect to obliquity (Drysdales et al., 2009).

Figure 6. Effect of **(a, b)** Greenland Ice Sheet elevation, insolation, albedo, and atmospheric methane concentration and **(c, d)** insolation and atmospheric methane concentration for the Last Interglacial (LIG) relative to preindustrial (PI). Model-data comparison of mean local summer temperature anomalies. The shading represents the simulated surface temperature (TS) anomalies at **(a, c)** 130 kyr BP derived from **(a)** LIG- 1300 m-alb and **(c)** LIG-ctl, and **(b, d)** summer maximum LIG warmth (warmest 100 warmest months between 130 and 120 kyr BP) derived from **(b)** LIG-1300m-alb-tr and **(d)** LIG-ctl-tr, relative to PI. Hatched areas in **(a, c)** mark statistically insignificant TS anomalies. The squares and circles show marine and terrestrial proxy-based maximum LIG summer temperature anomalies relative to PI derived by CAPE Last Interglacial Project Members (2006). The colors inside the squares and circles represent the proxy-based temperature anomalies derived from the intervals provided by CAPE Last Interglacial Project Members (2006), that agree best with the simulated TS anomalies at the location of the proxies.

Figure 7. Effect of **(a, b)** Greenland Ice Sheet elevation, insolation, albedo, and atmospheric methane

1 concentration and **(c, d)** insolation and atmospheric methane concentration for the Last Interglacial
2 (LIG) relative to preindustrial (PI). Model-data comparison of mean annual temperature anomalies. The
3 shading represents the simulated surface temperature (TS) anomalies at **(a, c)** 130 kyr BP derived from
4 **(a)** LIG-1300m-alb and **(c)** LIG-ctl, and **(b, d)** maximum LIG warmth (warmest 100 model years
5 between 130 and 120 kyr BP) derived from **(b)** LIG-1300m-alb-tr and **(d)** LIG-ctl-tr, relative to PI.
6 Hatched areas in **(a, c)** mark statistically insignificant TS anomalies. The squares and circles show
7 marine and terrestrial proxy-based LIG annual mean temperature anomalies relative to present-day
8 (1961–1990) derived by Turney and Jones (2010).

9
10 **Figure 8.** Effect of Greenland Ice Sheet elevation, insolation, albedo, and atmospheric methane
11 concentration for the Last Interglacial (LIG) relative to preindustrial (PI). **(a)** Proxy-based maximum
12 LIG summer temperature anomalies relative to PI derived by CAPE Last Interglacial Project Members
13 (2006) plotted against simulated local summer surface temperature (TS) anomalies at 130 kyr BP (LIG-
14 1300m-alb) relative to PI at the location of the proxies. The horizontal bars represent the proxy-based
15 temperature intervals derived by CAPE Last Interglacial Project Members (2006). The vertical bars
16 indicate the simulated TS anomalies at the maximum and minimum LIG TS with respect to local
17 summer (i.e. the coldest and warmest 100 warmest months) derived from the time interval 130 to 120
18 kyr BP (LIG-1300m-alb-tr) relative to PI, for each given proxy record location. **(b)** Proxy-based LIG
19 annual mean temperature anomalies relative to present-day (1961–1990) derived by Turney and Jones
20 (2010), plotted against simulated annual mean TS anomalies at 130 kyr BP (LIG-1300m-alb) relative to
21 PI at the location of the proxies. The vertical bars indicate the simulated TS anomalies at the maximum
22 and minimum LIG TS with respect to annual mean (i.e the coldest and warmest 100 model years)
23 derived from the time interval 130 to 120 kyr BP (LIG-1300m-alb-tr) relative to PI, for each given
24 proxy record location. **(c)** Same as **(b)** but displaying vertical bars that represent local summer and local
25 winter mean (i.e. the warmest 100 warmest months and coldest 100 coldest months). The squares (red)
26 and circles (black) represent marine and terrestrial proxy-based temperature anomalies, respectively.
27 The solid thick lines represent the 1 : 1 line that indicates a perfect match of simulated and
28 reconstructed anomalies.

29
30 **Figure 9.** Timing of the maximum Last Interglacial warmth for: **(a)** local summer (warmest 100
31 warmest months) and **(b)** annual mean (warmest 100 model years) derived from the LIG-1300m-alb-tr,

1 between 130 and 120 kyr BP.

2

3 **Figure 10.** Effect of **(a, b)** Greenland Ice Sheet elevation, insolation, albedo, and atmospheric methane
4 concentration and **(c, d)** insolation and atmospheric methane concentration at 130 kyr BP relative to
5 preindustrial (PI). Model-data comparison of mean local summer temperature anomalies. The shading
6 represents the simulated surface temperature (TS) anomalies derived from **(a, b)** LIG-1300m-alb and
7 **(c, d)** LIG-ctl. Hatched areas mark statistically insignificant TS anomalies. The squares show marine
8 proxy-based LIG (130 kyr BP) summer temperature anomalies relative to present-day derived by
9 Capron et al (2014).

10

11 **Figure 11.** Effect of **(a–c)** Greenland Ice Sheet elevation and **(c)** albedo on sea level pressure (SLP) and
12 surface winds in 130 kyr BP simulations. The shading represents December-January-February (DJF)
13 mean SLP anomalies, superimposed by DJF mean surface wind anomalies (in ms^{-1}) for: **(a)** LIG- $\times 0.5$
14 minus LIG-ctl, **(b)** LIG-1300m minus LIG-ctl, and **(c)** LIG-1300m-alb minus LIG-ctl. The vector
15 length indicates the wind speed (in ms^{-1}).

Simulation	Time (kyr BP)	CO ₂ (ppmv)	CH ₄ (ppbv)	N ₂ O (ppbv)	Greenland Ice Sheet	Veg.	e	ε (°)	ω (°)
LIG-ctl	130	278	650	270	PI	dyn.	0.0382	24.24	49.1
LIG-×0.5	130	278	650	270	×0.5	dyn.	0.0382	24.24	49.1
LIG-1300m	130	278	650	270	-1300m	dyn.	0.0382	24.24	49.1
LIG-1300m-alb	130	278	650	270	-1300m+alb	dyn.	0.0382	24.24	49.1
LIG-1300m-alb-CH ₄	130	280	760	270	-1300m+alb	dyn.	0.0382	24.24	49.1
LIG-GHG*	130	257	512	239	PI	PI	0.0382	24.24	49.1
LIG-125k*	125	278	650	270	-1300m+alb	dyn.	0.0400	23.79	128.1
PI	0	280	760	270	PI	dyn.	0.0167	23.45	282.2
LIG-ctl-tr	130-115	278	650	270	PI	dyn.	varying	varying	varying
LIG-×0.5-tr	130-115	278	650	270	×0.5	dyn.	varying	varying	varying
LIG-1300m-alb-tr	130-115	278	650	270	-1300m+alb	dyn.	varying	varying	varying
LIG-GHG-tr	130-115	varying	varying	varying	PI	PI	varying	varying	varying
HOL-tr	8-0	278	650	270	PI	dyn.	varying	varying	varying

Table 1

Simulation	AMOC (Sv)	Annual mean TS (°C)			Winter mean TS (°C)			Summer mean TS (°C)		
		global	NH	SH	global	NH	SH	global	NH	SH
LIG-ctl	12.8	14.77	15.57	13.98	8.76	6.53	10.98	21.00	24.78	17.22
LIG-×0.5	13.3	15.13	16.03	14.22	9.19	7.12	11.25	21.25	25.09	17.41
LIG-1300m	14.8	15.07	15.95	14.18	9.14	7.05	11.22	21.17	24.96	17.39
LIG-1300m-alb	15.0	15.14	16.00	14.29	9.24	7.10	11.37	21.24	25.02	17.46
LIG-1300m-alb-CH ₄	14.4	15.32	16.34	14.29	9.40	7.49	11.31	21.43	25.35	17.50
LIG-GHG	12.8	14.65	15.50	13.80	8.69	6.56	10.82	20.82	24.64	17.00
LIG-125k	14.8	15.19	16.11	14.27	9.46	7.74	11.17	21.20	24.94	17.46
PI	16.3	14.51	15.35	13.67	8.84	7.44	10.23	20.09	22.84	17.33

Table 2

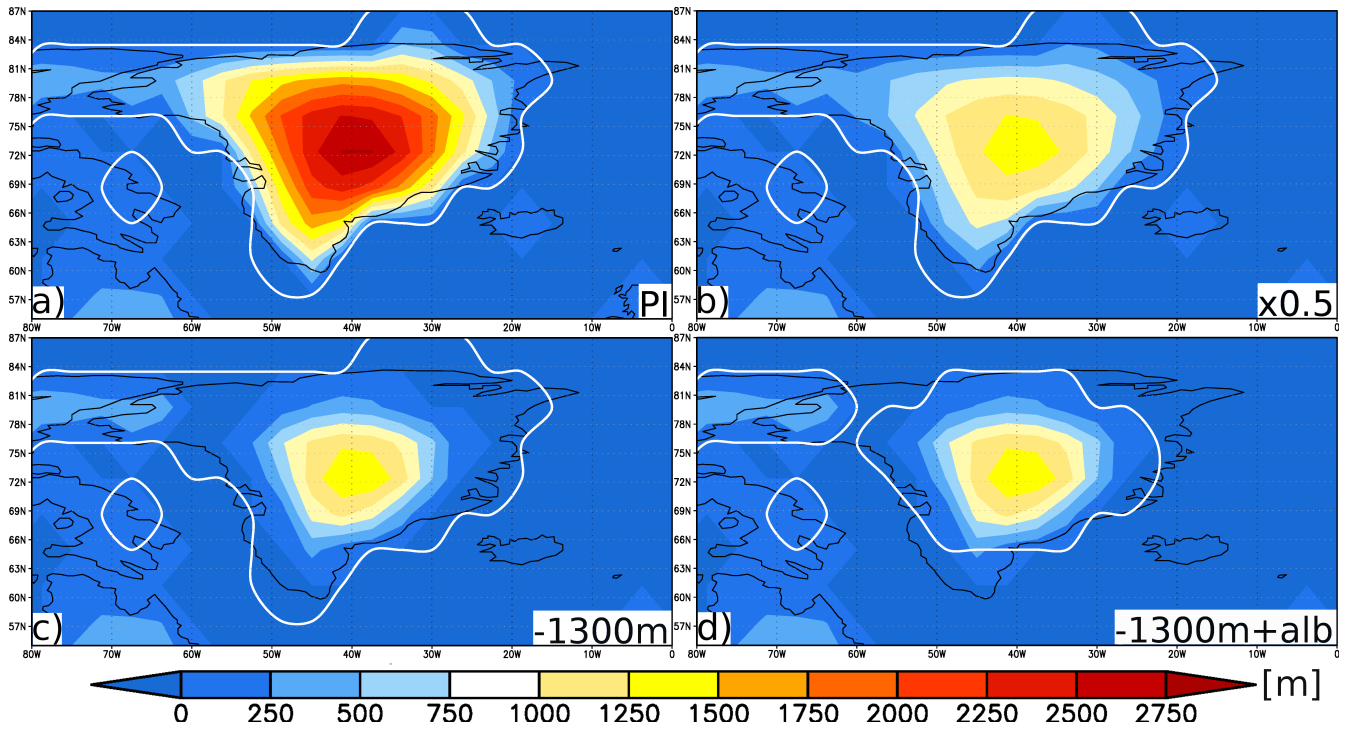


Figure 1

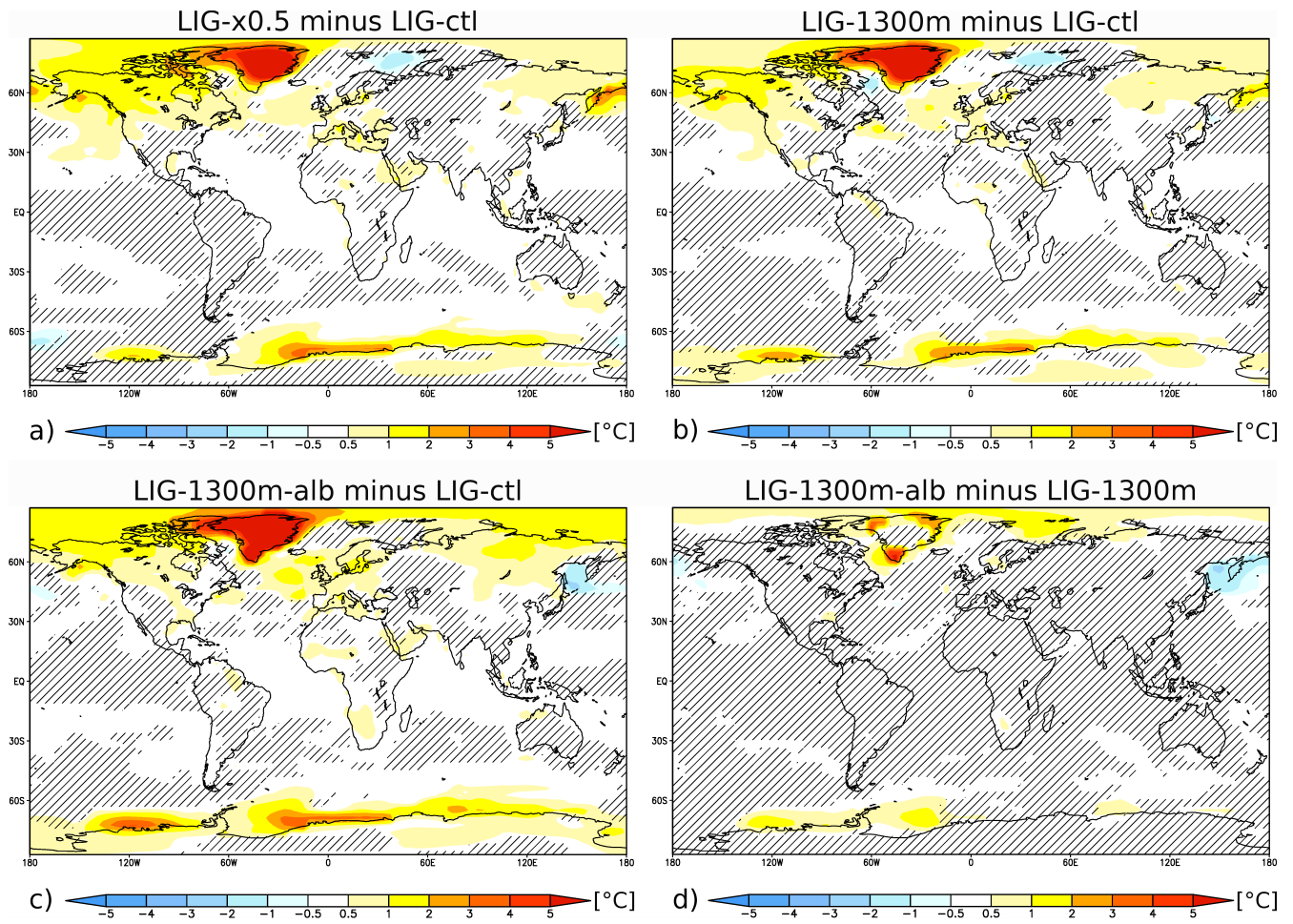
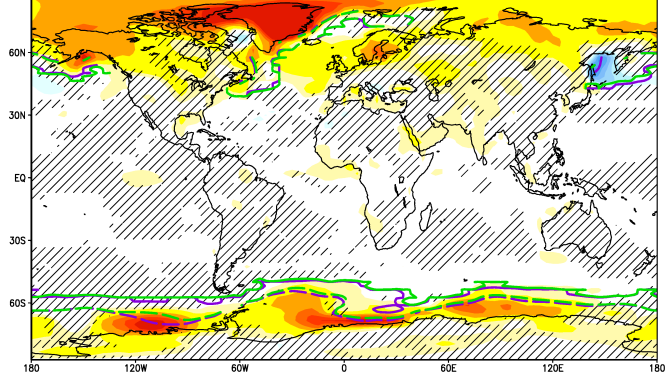


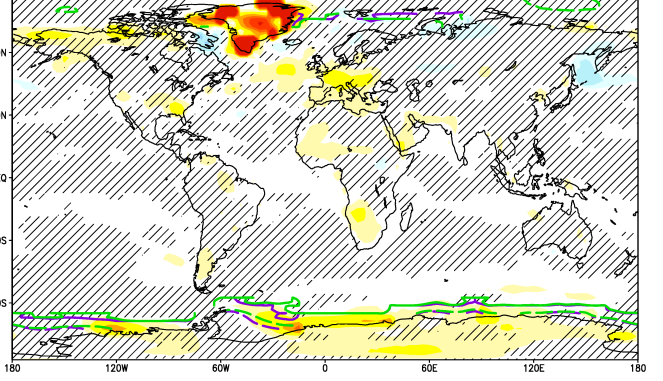
Figure 2

LIG-1300m-alb minus LIG-ctl (local winter)



a) [°C]

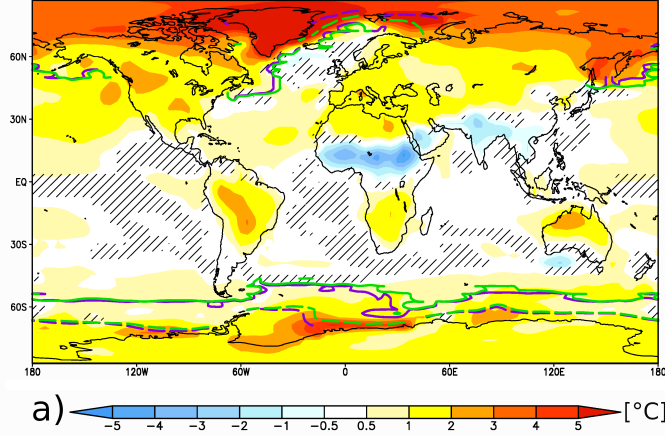
LIG-1300m-alb minus LIG-ctl (local summer)



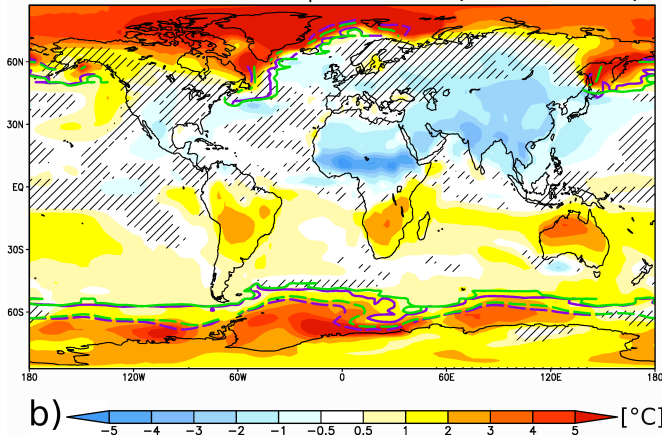
b) [°C]

Figure 3

LIG-1300m-alb-CH₄ minus PI (annual mean)



LIG-1300m-alb-CH₄ minus PI (local winter)



LIG-1300m-alb-CH₄ minus PI (local summer)

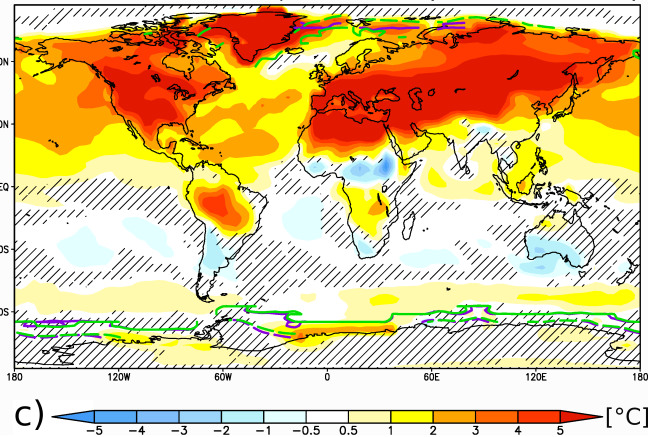


Figure 4

Northern high latitudes (60-90°N)

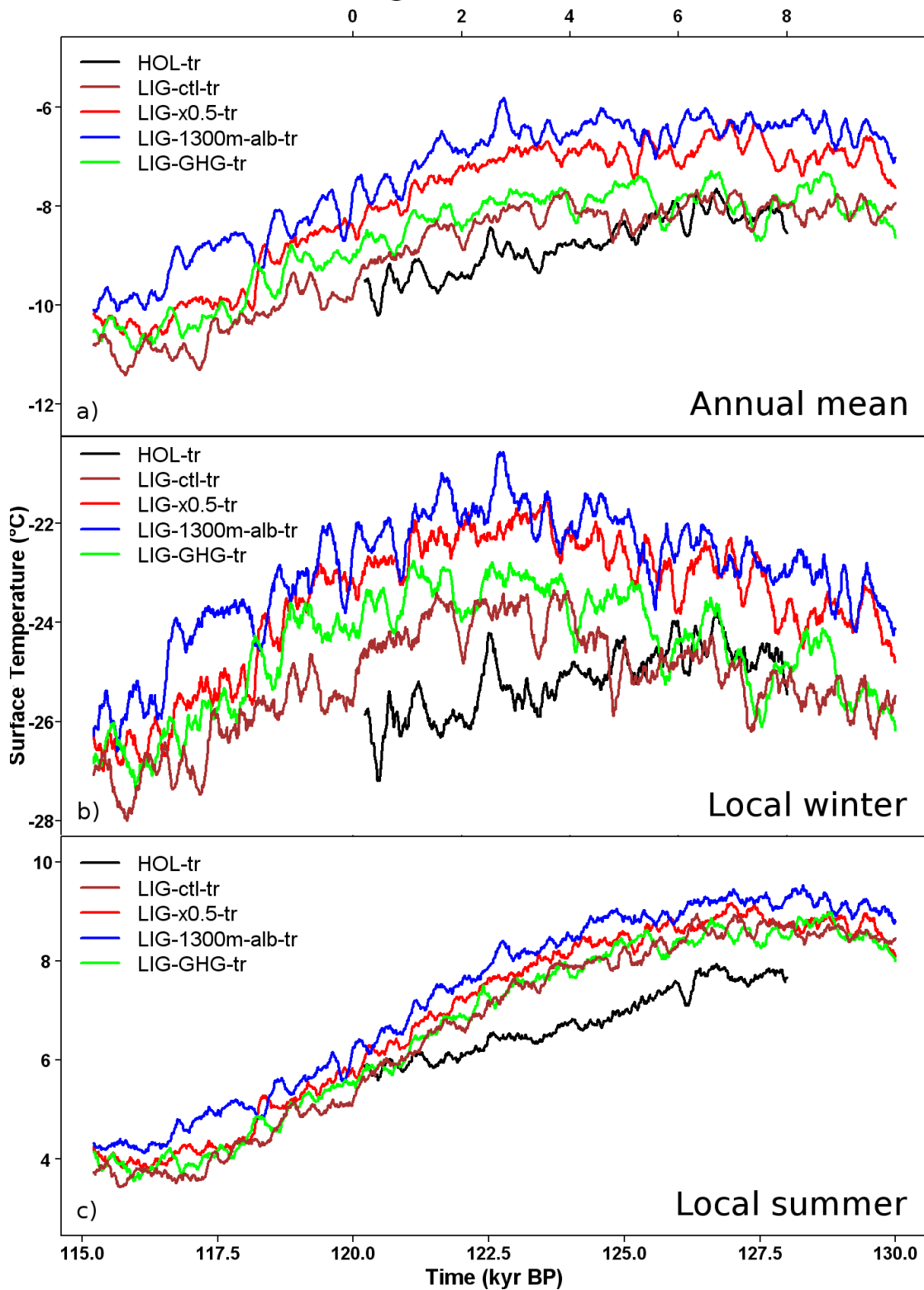
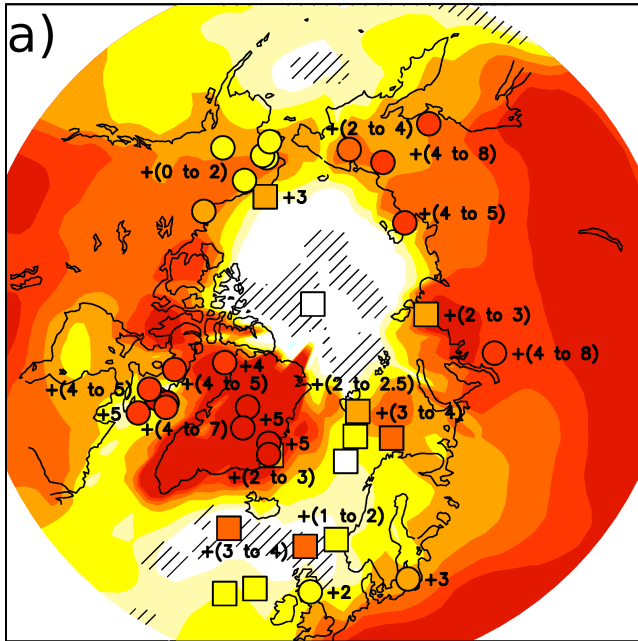


Figure 5

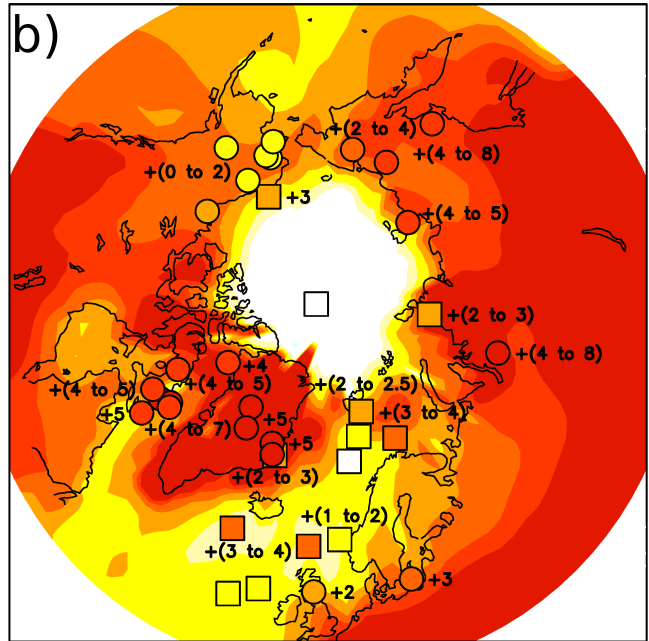
Local summer at 130 kyr BP

LIG-1300m-alb minus PI

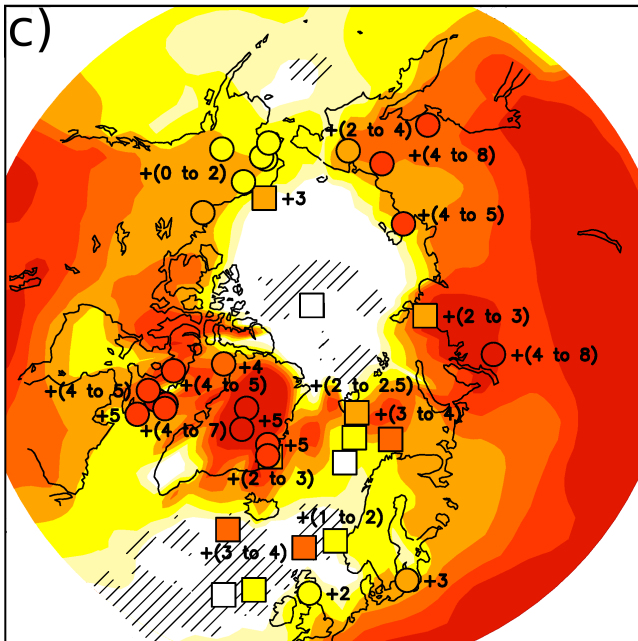


Local summer at maximum LIG warmth

LIG-1300m-alb-tr minus PI



LIG-ctl minus PI



LIG-ctl-tr minus PI

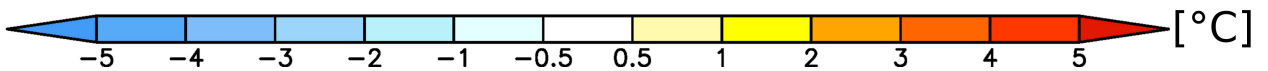
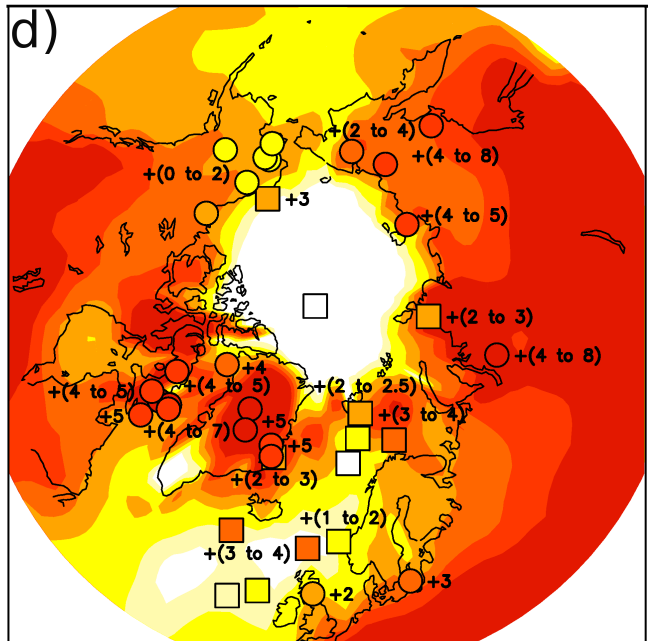
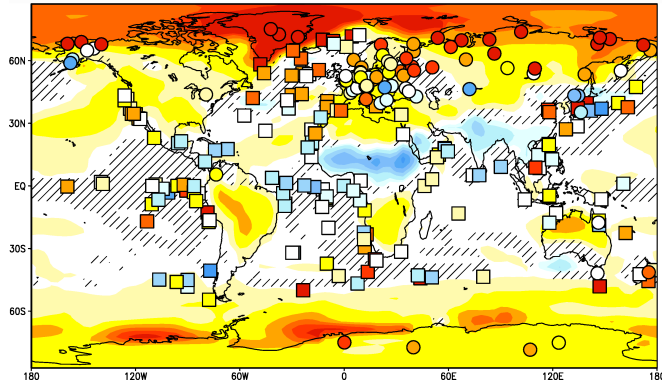
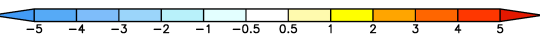


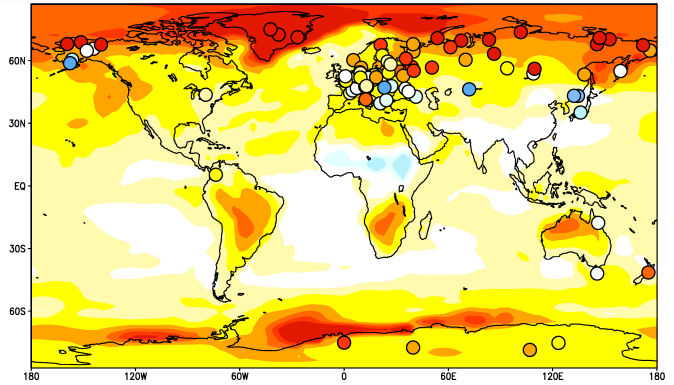
Figure 6

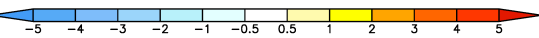
Annual mean at 130 kyr BP
LIG-1300m-alb minus PI



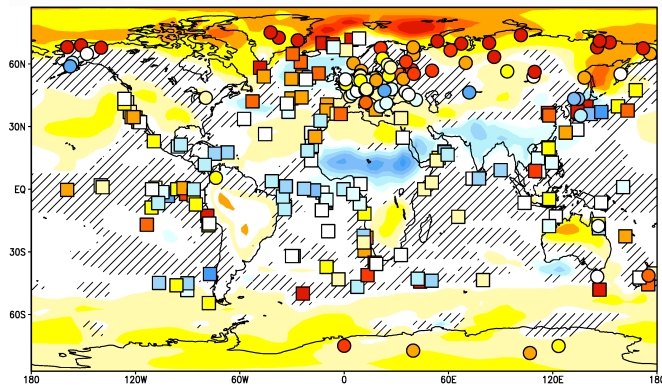
a)  [°C]

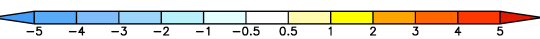
Annual mean at maximum LIG warmth
LIG-1300m-alb-tr minus PI



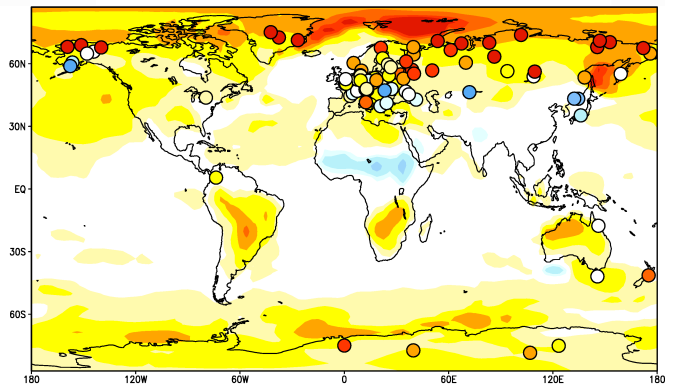
b)  [°C]

LIG-ctl minus PI



c)  [°C]

LIG-ctl-tr minus PI



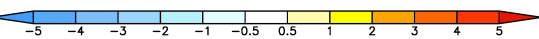
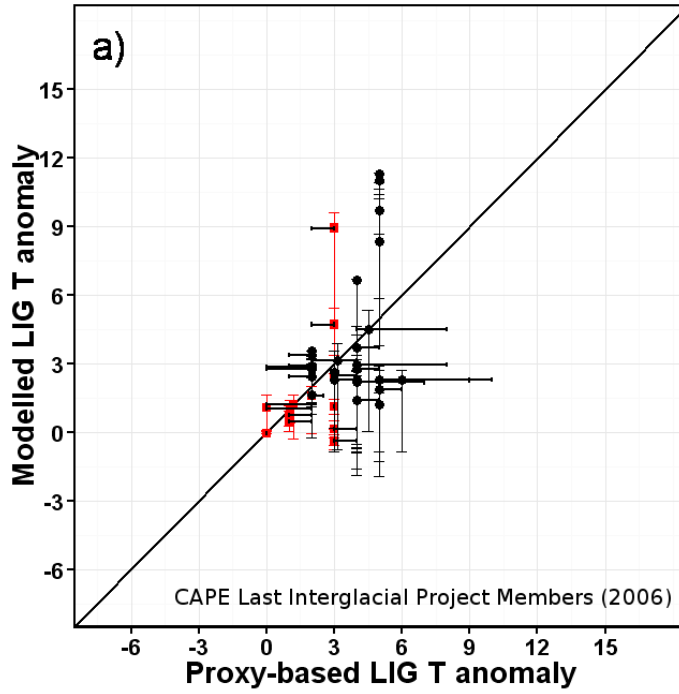
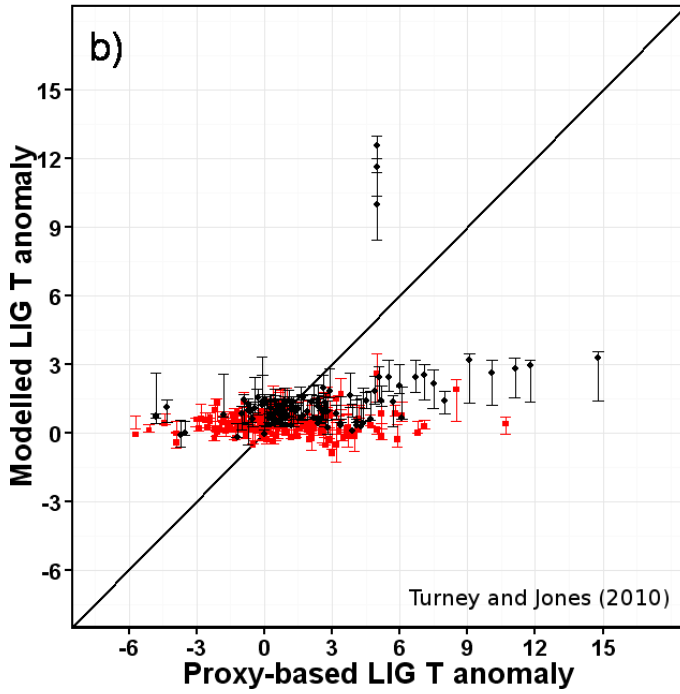
d)  [°C]

Figure 7

Proxy vs. simulated local summer [°C]



Proxy vs. simulated annual mean [°C]



Proxy vs. simulated annual mean, local winter and summer [°C]

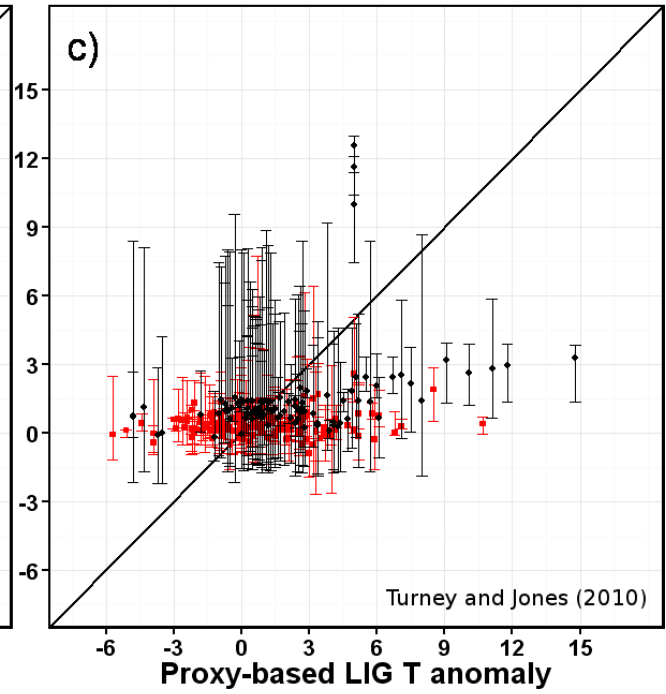


Figure 8

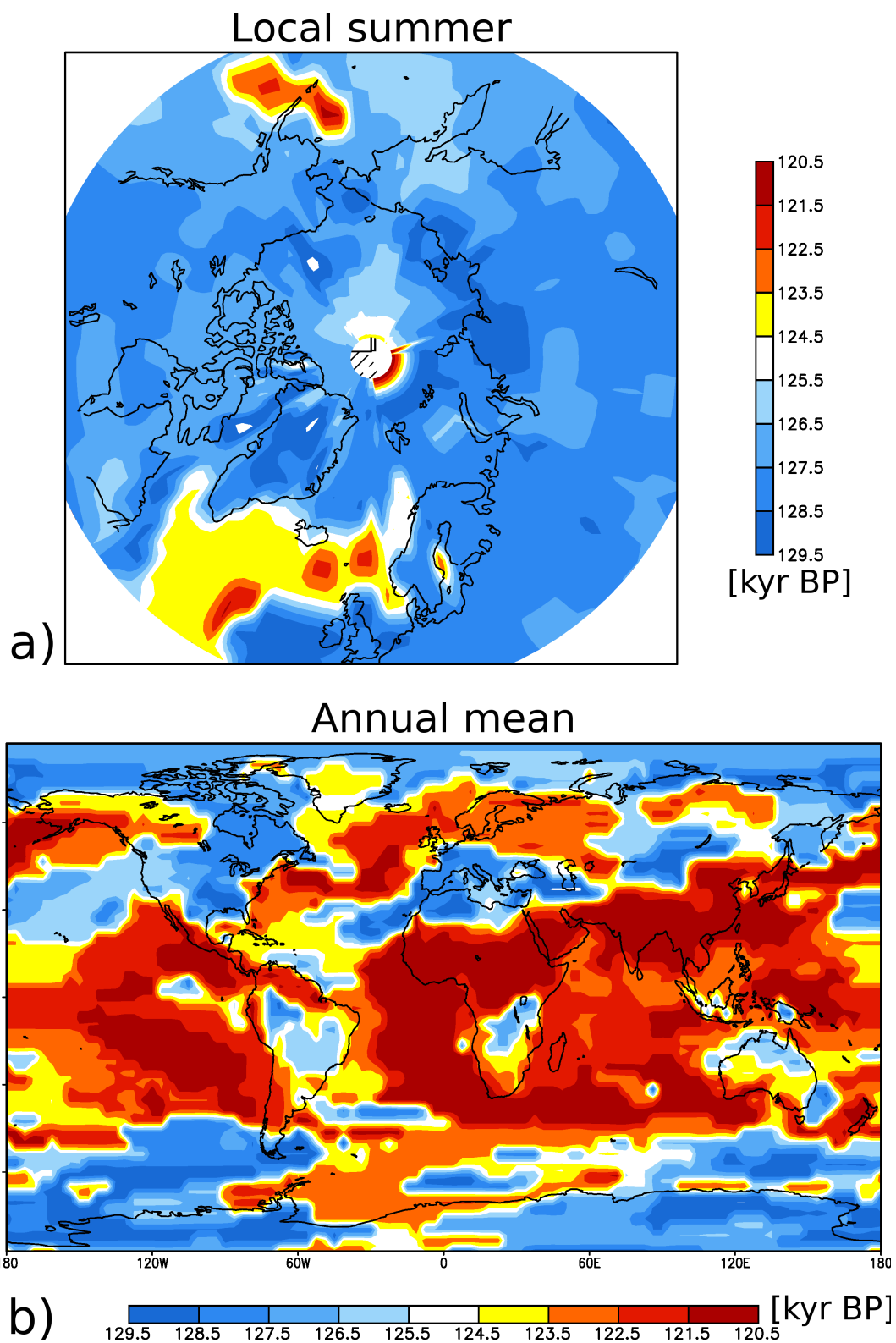
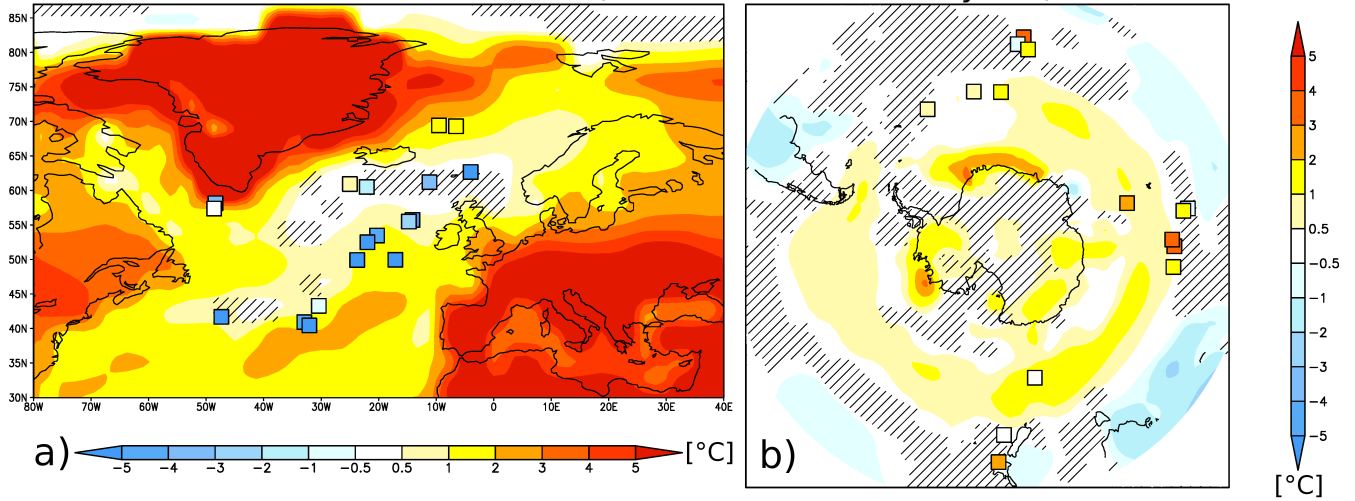


Figure 9

LIG-1300m-alb minus PI (local summer at 130 kyr BP)



LIG-ctl minus PI (local summer at 130 kyr BP)

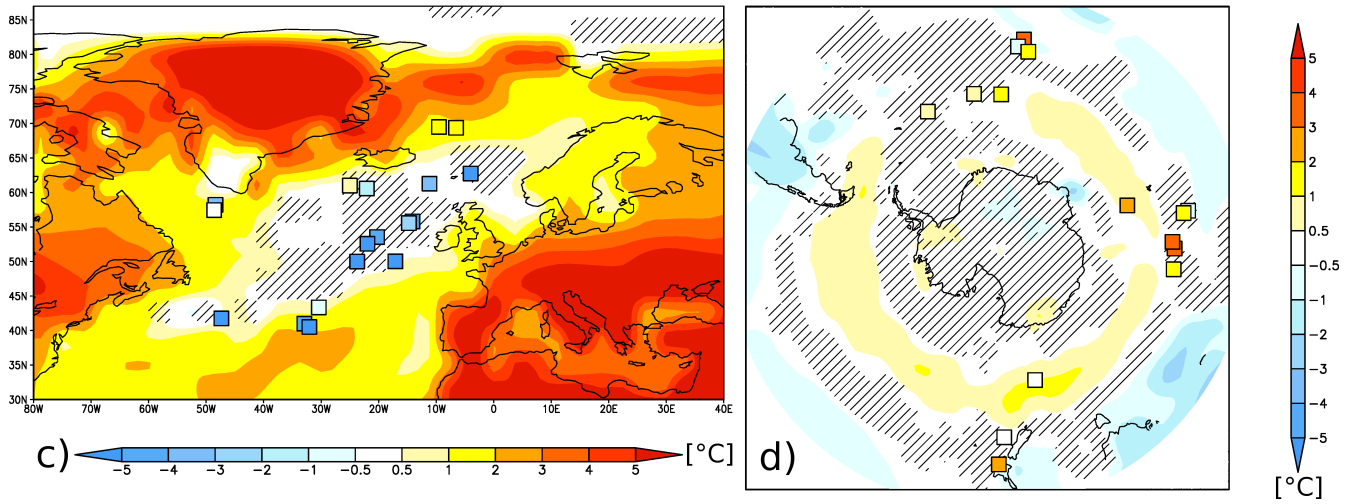


Figure 10

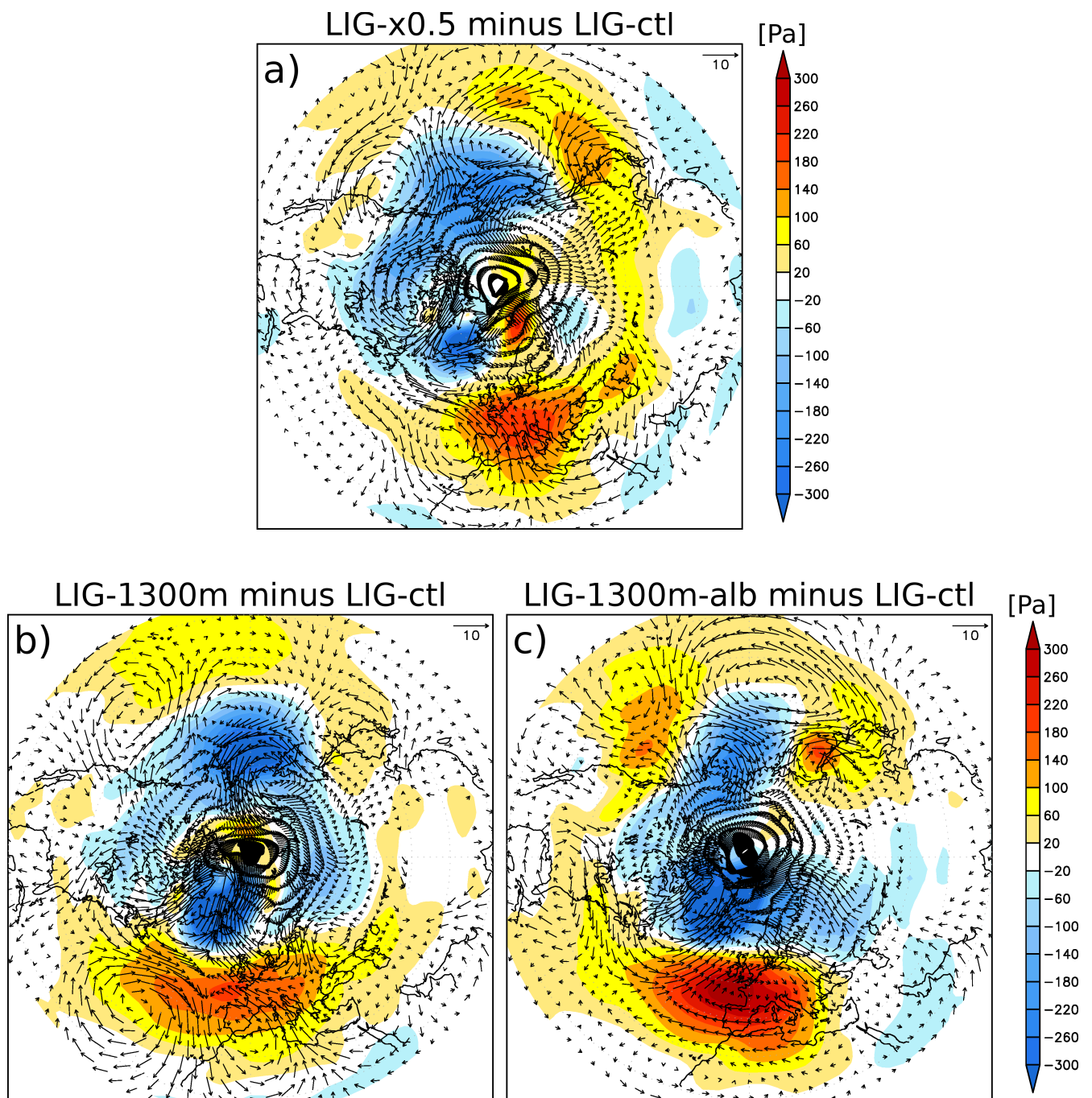


Figure 11